

Review

# Microfluidic-Based Oxygen (O<sub>2</sub>) Sensors for On-Chip Monitoring of Cell, Tissue and Organ Metabolism

Mostafa Azimzadeh <sup>1,2,3</sup> , Patricia Khashayar <sup>4</sup> , Meitham Amereh <sup>5,6,7</sup> , Nishat Tasnim <sup>7</sup> , Mina Hoorfar <sup>7,\*</sup> and Mohsen Akbari <sup>5,6,8,\*</sup> 

- <sup>1</sup> Medical Nanotechnology & Tissue Engineering Research Center, Yazd Reproductive Sciences Institute, Shahid Sadoughi University of Medical Sciences, Yazd 89195-999, Iran; m.azimzadeh@ssu.ac.ir
  - <sup>2</sup> Stem Cell Biology Research Center, Yazd Reproductive Sciences Institute, Shahid Sadoughi University of Medical Sciences, Yazd 89195-999, Iran
  - <sup>3</sup> Department of Medical Biotechnology, School of Medicine, Shahid Sadoughi University of Medical Sciences, Yazd 89165-887, Iran
  - <sup>4</sup> Center for Microsystems Technology, Imec and Ghent University, 9050 Ghent, Belgium; patricia.khashayar@ugent.be
  - <sup>5</sup> Laboratory for Innovations in Micro Engineering (LiME), Department of Mechanical Engineering, University of Victoria, Victoria, BC V8P 5C2, Canada; mamereh@uvic.ca
  - <sup>6</sup> Center for Advanced Materials and Related Technologies, University of Victoria, Victoria, BC V8P 5C2, Canada
  - <sup>7</sup> Department of Mechanical Engineering, University of Victoria, Victoria, BC V8P 5C2, Canada; nishattasnim@uvic.ca
  - <sup>8</sup> Biotechnology Center, Silesian University of Technology, Akademicka 2A, 44-100 Gliwice, Poland
- \* Correspondence: mhoorfar@uvic.ca (M.H.); makbari@uvic.ca (M.A.)

**Abstract:** Oxygen (O<sub>2</sub>) quantification is essential for assessing cell metabolism, and its consumption in cell culture is an important indicator of cell viability. Recent advances in microfluidics have made O<sub>2</sub> sensing a crucial feature for organ-on-chip (OOC) devices for various biomedical applications. OOC O<sub>2</sub> sensors can be categorized, based on their transducer type, into two main groups, optical and electrochemical. In this review, we provide an overview of on-chip O<sub>2</sub> sensors integrated with the OOC devices and evaluate their advantages and disadvantages. Recent innovations in optical O<sub>2</sub> sensors integrated with OOCs are discussed in four main categories: (i) basic luminescence-based sensors; (ii) microparticle-based sensors; (iii) nano-enabled sensors; and (iv) commercial probes and portable devices. Furthermore, we discuss recent advancements in electrochemical sensors in five main categories: (i) novel configurations in Clark-type sensors; (ii) novel materials (e.g., polymers, O<sub>2</sub> scavenging and passivation materials); (iii) nano-enabled electrochemical sensors; (iv) novel designs and fabrication techniques; and (v) commercial and portable electrochemical readouts. Together, this review provides a comprehensive overview of the current advances in the design, fabrication and application of optical and electrochemical O<sub>2</sub> sensors.

**Keywords:** oxygen sensors; microfluidics; organ-on-chips (OOCs); on-chip monitoring



**Citation:** Azimzadeh, M.; Khashayar, P.; Amereh, M.; Tasnim, N.; Hoorfar, M.; Akbari, M. Microfluidic-Based Oxygen (O<sub>2</sub>) Sensors for On-Chip Monitoring of Cell, Tissue and Organ Metabolism. *Biosensors* **2022**, *12*, 6. <https://doi.org/10.3390/bios12010006>

Received: 4 November 2021

Accepted: 14 December 2021

Published: 22 December 2021

**Publisher's Note:** MDPI stays neutral with regard to jurisdictional claims in published maps and institutional affiliations.



**Copyright:** © 2021 by the authors. Licensee MDPI, Basel, Switzerland. This article is an open access article distributed under the terms and conditions of the Creative Commons Attribution (CC BY) license (<https://creativecommons.org/licenses/by/4.0/>).

## 1. Introduction

Oxygen (O<sub>2</sub>) is one of the main components of cellular respiration and energy production [1]. The availability of O<sub>2</sub> is a key metric that defines the pathway of adenosine triphosphate (ATP) generation and its resultant metabolites that serve as the living cell's energy source [2,3]. In a high O<sub>2</sub> environment, ATP is synthesized by the phosphorylation of the precursor molecule adenosine diphosphate (ADP). This process, thus called aerobic respiration, requires an adequate level of O<sub>2</sub>. It consists of the coupling of electron transport and oxidative phosphorylation, where O<sub>2</sub> acts as the final electron acceptor from the oxidation of glucose and/or glycogen [4]. In low O<sub>2</sub> environments, conversely, ATP is generated at an inefficient but rapid rate via a process called anaerobic glycolysis, where glucose and glycogen are metabolized to pyruvate and lactate in the absence of O<sub>2</sub>. This

pathway is important in the functions of vital organs such as the kidney and retina as well as in tumor formation [5]. O<sub>2</sub> availability determines the metabolic pathway that generates energy for cell function and survival and therefore is significantly important to measure for bioassays, cell culture and diagnostic applications.

Precise control of a small amount of fluid is possible inside microfabricated channels of microfluidic technology [6]. Integrated microfluidic chips are capable of performing highly sensitive and low-cost analyses. These platforms can be integrated with new technologies with cell culture/organoid studies at high temporal and spatial resolution. For instance, microfluidic platforms can quantitatively monitor cellular signals and cell secretions using well-developed cell-culture methods on microchips [7]. O<sub>2</sub> measurement can be performed using sensors integrated into microfluidic chips for monitoring the metabolism and viability of cell, tissue, and organ [8,9]. Moreover, novel sensors embedded inside implantable microchips have recently been used for real-time *in vivo* oximetry in human or animal bodies [10]. Sensors can also be used to detect and quantify various analytes in a complex biological environment [11–16]. Therefore, a combination of integrated sensors is required for online and non-invasive monitoring of the cell intake, secreted metabolites, and microenvironment status for on-chip microfluidic studies such as OOC and bioreactors [12,13].

On-chip monitoring of O<sub>2</sub> is pivotal in OOCs. The low concentration of O<sub>2</sub> inside a small chip and its crucial biological role in cell metabolism and function would emphasize the need for its precise and selective quantification in the confined environment of a microfluidic channel or chamber [9,17]. With recent advances in microfluidics-based cell and tissue studies, such as OOC technologies, various sensors have been integrated into chips to monitor the microphysiological parameters of cells [12,18–23]. OOCs have the potential to better mimic human organs compared to the traditional *in vitro* models, and thus they can reduce the need for animal models in interventions such as the studies on drug efficacy and toxicity [24–26]. To model the function of many organs, such as the pancreas [27], brain [28–30], liver [31], vascular system [32], Gut [33], multiorgan approaches [34] and body-on-the-chip, OOC-integrated O<sub>2</sub> sensing techniques have been used to culture cell monolayers, three dimensional (3D) cultures, spheroids, organoids and stem cells. They have also been used to model tumor microenvironment by mimicking the extracellular matrix (ECM) [35] and 3D culture of cancer cells [36,37].

Electrochemical and optical sensors are the main transducers for on-chip O<sub>2</sub> monitoring [38], as they are precise, selective, and easy to miniaturize and implement inside chips [18,39]. In addition, micro and nanomaterials along with the innovative designs and polymers, and commercial readout devices are used for signal amplification to overcome the limitation related to the measurement of low O<sub>2</sub> levels with electrochemical and optical sensors [13,40,41]. Here, we review the recent innovations in O<sub>2</sub> sensors integrated into microfluidic chips, including OOC devices. We have categorized them based on their transducer type into two main sections, namely optical and electrochemical. We also discuss recent innovations and their advantages and disadvantages. Finally, we provide a comprehensive discussion of the current advances in the design, fabrication and application of optical and electrochemical O<sub>2</sub> sensors.

Previous reviews have covered related topics such as oxygen control (2016) [9], general optical imaging and sensing (2014) [39], microfluidic OOC sensors (2010) [40], and other microphysiological sensors of OOCs [12,13,18,38]; however, there are no recent publications critically discussing the current advancements in OOC O<sub>2</sub> sensing. The present review delves into a critical examination of recent developments in O<sub>2</sub> sensors integrated into OOCs devices and provides a comprehensive comparison of their advantages, limitations and required future improvements.

## 2. Oxygen Sensors in On-Chip Systems

Methods of on-chip O<sub>2</sub> measurement can be categorized into two groups of sensors: (i) optical and (ii) electrochemical. Here, we highlight the application of these two types of

sensors in on-chip studies, explain their mechanism of action, and discuss their advantages and disadvantages. Table 1 represents the summary of advantages and disadvantages of optical and electrochemical methods for on-chip O<sub>2</sub> measurement.

**Table 1.** Comparison of chip-based electrochemical and optical O<sub>2</sub> sensors.

Method	Advantages	Limitations
Optical	<ul style="list-style-type: none"> <li>• Precise, sensitive and selective</li> <li>• Easy to miniaturize</li> <li>• Nano and microparticles for dye protecting</li> <li>• Non-invasive, and contact-free</li> <li>• Easy to use and operate</li> <li>• Commercial dyes and read-out devices</li> <li>• Simple handling and sterilizing of the chip</li> <li>• Less need to recalibrate</li> <li>• Multiplex measurement in different chip spots</li> <li>• Simultaneously measure pH and metabolites</li> </ul>	<ul style="list-style-type: none"> <li>• Complicated integration into the chip</li> <li>• Possible dyes bleaching</li> <li>• Sometimes needs microscope</li> </ul>
Electrochemical	<ul style="list-style-type: none"> <li>• Precise, sensitive and selective</li> <li>• Easily miniaturized/implemented inside chips</li> <li>• Nano and microparticles for dye protecting</li> <li>• Possible use of commercial read-out devices</li> <li>• Short response time</li> <li>• High sensitivity</li> <li>• Label-free</li> <li>• Several electrodes</li> <li>• Several surface modifications</li> <li>• Several designs and polymers can be used easily</li> </ul>	<ul style="list-style-type: none"> <li>• Invasive and consume oxygen</li> <li>• Expensive integration in the chip</li> <li>• Requires special instrument and skilled operators</li> </ul>

### 2.1. Optical Methods

Optical strategies for O<sub>2</sub> sensing have been widely used in on-chip systems. Luminescent sensors are the most common type of these sensors that utilize either fluorescence or phosphorescence dyes that respond to O<sub>2</sub> molecules as a quencher available inside the chip. Optical methods have been used more than electrochemical methods for on-chip O<sub>2</sub> sensing due to their lower limit of detection ranges, lower cost and ease of manufacturing. They have great potential to be used as a portable point-of-need detection and connecting to commercial optical measurement (readout) devices. The advantage of the optical sensing technique is that O<sub>2</sub> is not consumed during the optical measurement, unlike other methods. Additionally, optical fibers can measure O<sub>2</sub> levels easier without the need of direct contact of the culture media by adding a protecting layer of oxygen diffusing materials, such as PDMS, on the optical fiber. This feature is beneficial for keeping the cell microenvironment intact or when O<sub>2</sub> content or resource is limited. Optical O<sub>2</sub> measurements can also be simultaneously performed with the measurement of other important parameters, such as pH and cell metabolites (such as lactate, glucose, and amino acids) [9,12,38,39].

In the following sections, we summarize the advancements in optical O<sub>2</sub> sensors four main categories based on their type of innovations. Furthermore, to make the comparison easier, Table 2 represents the summary of most recent on-chip optical O<sub>2</sub> sensors and their features, applied dyes, and their advantages.

**Table 2.** Characteristics of chip-based optical O<sub>2</sub> sensors.

Optical O <sub>2</sub> Sensor	Application	Dye	Advantages	References
Polystyrene chip, pore network structure, used solvent-induced fluorophore impregnation (SIFI) method for dye layer	Cell	PtTFPP	Enhanced sensitivity and stability, non-invasive, can be used for gas and dissolved O <sub>2</sub>	[41]
PDMS chip with glass layer coverage, applied oxygen gradient	Liver	PtOEP	Wide dynamic range, continuous measurement, non-invasive, worked in different flow rates	[42]
Cyclic olefin copolymer-based chip	Lung	PtTPTBPF	Simultaneous O <sub>2</sub> and pH, stop/flow measurements, long term stability (10 days), non-invasive	[43]
PDMS chip, applied oxygen gradient	Cancer	PtOEPK	Photostable, reusable, non-invasive	[44]
PDMS chip, silica microparticles	Cancer	Ru(dpp)	Simple fabrication and handling, real-time, spatially-resolved measurements, low photobleaching, High sensitivity	[45]
PMMA chip, polystyrene microspheres	Embryo study	Pt-porphyrin	Simultaneous O <sub>2</sub> and pH, long-term measurement, highly sensitive for single embryo analysis	[46]
PDMS chip, polystyrene microbeads	Liver	ruthenium-phenanthroline (RuP)	Every 15 min for 28 days measurement, without a decrease in signal loss and toxicity, simultaneous glucose and lactate measurements	[47]
Glass chip, nanoparticle probes	Stem cell	PtTFPPBr <sub>2</sub>	Highly sensitive, real-time, label-free, high-intensity fluorescence emission, cell permeability	[48]
Teflon fluorinated ethylene propylene (FEP) tubing, poly(styrene-block-vinylpyrrolidone) nanobeads	Bacteria	PtTPTBPF	Minimized background fluorescence, simultaneous measurement, highly soluble and disperse nanobeads, prevents any interferences from biomolecules, short response times, no dye leaching, and long storage periods	[49]
Silicon/glass chip, core–shell nanosensors (poly(styrene-blockvinylpyrrolidone))	Fibroblast cell	PtTPTBPF	Simultaneous O <sub>2</sub> and pH, contactless and inexpensive read-out, high ionic strength, highly stable, online monitoring	[50]
Glass chip, polymeric nanoparticles	Cell	Pt(II) benzoporphyrin	Highly stable at different pH, ultrafast response (less than 0.2 s), no leaching, repeatable	[51]

### 2.1.1. Basic Luminescence-Based Sensors

The luminescence-based sensing method relies on quenching of luminescence (fluorescence or phosphorescence) dyes by O<sub>2</sub> molecules based on the Stern-Volmer equation [39], which reflects the relationship between the concentration of O<sub>2</sub> and fluorescent intensity [52,53]. Dyes are mixed with polymers containing O<sub>2</sub> permeable and soluble features to make a sensing layer on chip where the emission readout will be measured following an excitement in specific spectra. The main advantages of this strategy are its high sensitivity and selectivity toward O<sub>2</sub>, ease of fabrication, high photo-stability (suitable for long-term and continuous O<sub>2</sub> monitoring), and short response time (typically less than a few seconds) [52–54].

The most popular dyes used for O<sub>2</sub> sensing include metal–ligand complexes, particularly metalloporphyrins [39]. These dyes are photostable with sharp, strong luminescent

signals that can be excited in the visible spectrum. Moreover, small changes in their structure (peripheral substitution) can alter their chemical and spectroscopic properties, suggesting that they are tunable. Due to the longer lifetime of their excitement, their quenching efficacy is high. Therefore, they have high O<sub>2</sub> sensing sensitivity [39,44,55,56]. Few examples of the most used dyes are Platinum(II) tetrakis(pentafluorophenyl)porphyrin (PtTFPP) [57], Platinum (II) octaethylporphyrin (PtOEP) [42], Platinum (II)-meso-tetra(4-fluorophenyl)tetrabenzoporphyrin (PtTPTBPF) [43], Ruthenium-tris(4,7-diphenyl-1,10-phenanthroline) dichloride (Ru(dpp)) [55], and Singlet O<sub>2</sub> sensor green (SOSG) [56]. In a few studies, other materials such as polymerized 2-hydroxyethyl methacrylate (HEMA) have been used as a dye [58].

The dyes are mostly embedded into dye-impregnated polymeric layers at the vicinity of the cell chambers during the fabrication of chips. The layers are developed by directly mixing or dissolving the dyes into the solvent or polymer and then forming a film layer inside or at the top of the microfluidic channels and chambers [59]. Impregnated polymers are then patterned into the cell chambers using spin coating [44], knife coating [60], and preheated coating dye solution [41]. Dyes are excited by either light-emitting diode (LEDs) or optical fibers. The signal readout is achieved by using Charge-Coupled Devices (CCD) camera [61], fluorescent microscope imaging [42] (Figure 1A) or via optical fibers [43] (Figure 1B). To quantify the signal in real-time, the collected optical signal is converted into an electrical signal using a designed detection circuitry with output monitoring and data collection components [13,55]. An alternative strategy of ratiometric O<sub>2</sub> sensing has been employed in recent studies to improve the readout, defined as the ratio of the O<sub>2</sub>-sensing dye readout signal or image to the non-O<sub>2</sub> sensitive reference dye signal. Figure 1C shows an example of the ratiometric concept, where the standard deviation is proved to be half of the typical imaging intensity-based strategies [61]. In addition, few studies have used phosphorescence for on-chip O<sub>2</sub> sensing, using the previously described luminescent dyes with longer excited-state lifetimes [62]. In these studies, the dyes were utilized for phosphorescence sensing of O<sub>2</sub> with the same concept used in filmmaking strategies for luminescent methods [62–64].

One of the main ways to enhance the sensitivity and stability of the optical O<sub>2</sub> measurement is via the fabrication techniques such as solvent-induced fluorophore impregnation (SIFI) method [41]. The method was recently developed which involves the impregnation of PtTFPP dye into the body of the cell culture chip without adding a dye-coating inside the chip. In this strategy, the challenges associated with patterning sensing layers in chambers, such as delamination and formation of cracks, were eliminated [41]. The application of optical fibers in O<sub>2</sub> sensing has several advantages including the possibility for online and remote monitoring and miniaturization in O<sub>2</sub> sensing devices [65,66]. Additionally, Yang and colleagues developed a capillary optical fiber (COF) with a ring-shaped waveguide used for O<sub>2</sub> detection. They coated luminescent dyes on the inner surface of the waveguide in the COF for ratiometric O<sub>2</sub> measurement with high sensitivity (high ratio of O<sub>2</sub>-sensitive dye signal over the control dye) and low response time (less than 7s). However, the main drawbacks of this method are the high cost and the need for special readout devices [67]. In many cases, O<sub>2</sub> measurement needs to be performed simultaneously along other important parameters such as pH and cell metabolites to assess cell physiological condition. This can be carried out by several techniques such as using different dyes [43,58], micro-patterning the sensors in various layers of the chip [42], using optical fibers that have several excitation/emission wavelengths corresponding to O<sub>2</sub> and pH [43] (Figure 1B).

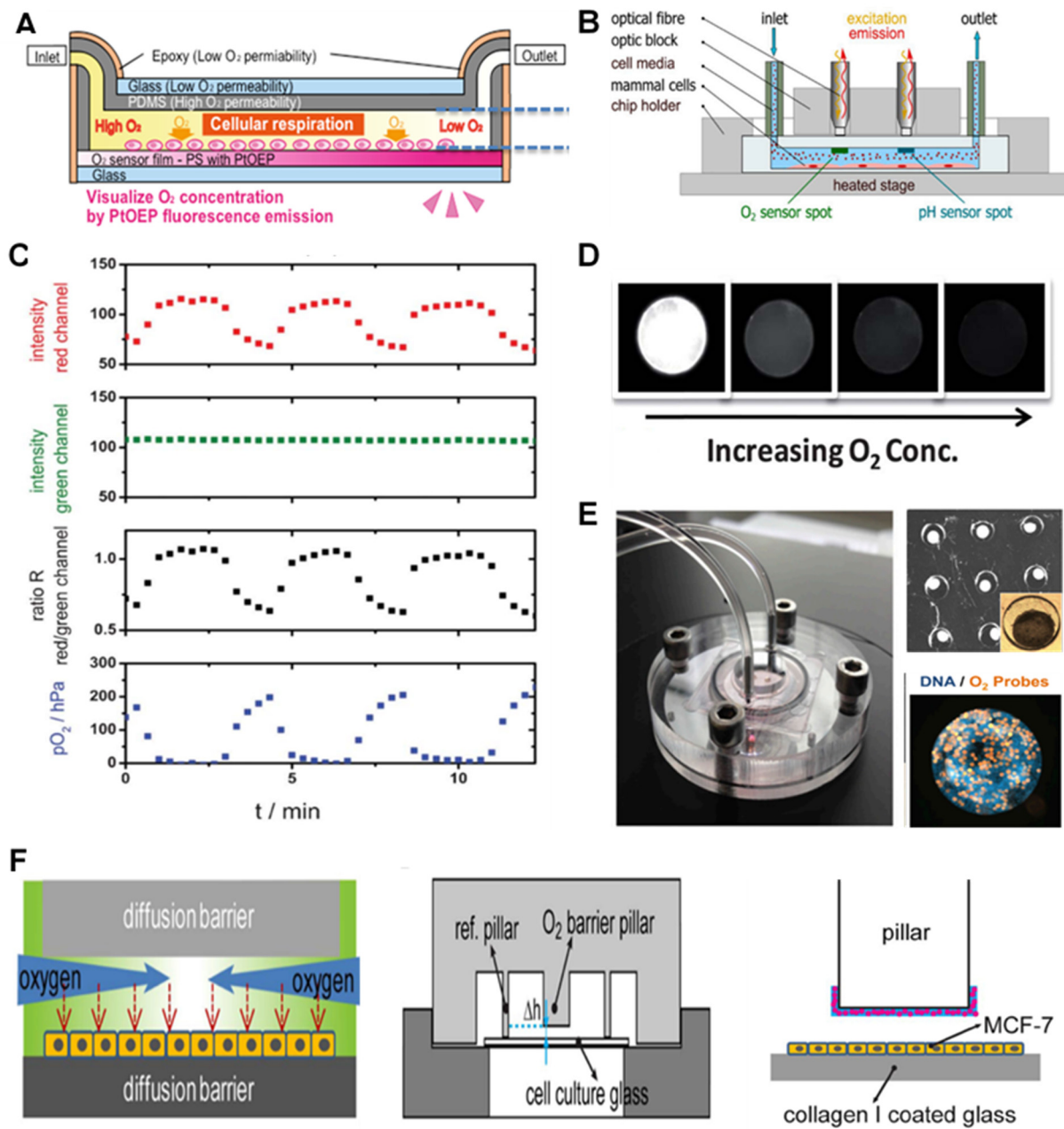


**Figure 1.** Basic luminescence-based sensors and microtechnology-based luminescent sensors for O<sub>2</sub> monitoring in on-chip studies. (A) The concept of an integrated layer of O<sub>2</sub>-sensitive dye in an OOC device for liver studies. Reproduced with permission [42], copyright 2019, John Wiley & Sons. (B) Optical fiber-based detection of O<sub>2</sub> and pH. Reproduced with permission [43], copyright 2021, Elsevier. (C) The ratiometric concept for optical O<sub>2</sub> sensing through comparing the signals from O<sub>2</sub>-sensitive dyes with that of non-O<sub>2</sub> sensitive ones as reference. Reproduced with permission [61], copyright 2013, The Royal Society of Chemistry. (D) PDMS Microbeads containing luminescent dyes were synthesized using microfluidics for O<sub>2</sub> sensing. Their performance in an O<sub>2</sub> gradient (different concentrations of O<sub>2</sub>) is represented. Reproduced with permission [68], copyright 2012, The Royal Society of Chemistry. (E) A bioreactor (liver-on-chip) device (left) for the analysis of drug effect on mitochondrial activity of the HepG2/C3A organoids. Each microwell contains an organoid (top right) with integrated microparticles with luminophores for imaging-based O<sub>2</sub> sensing (right). Reproduced with permission [69], copyright 2016, National Academy of Sciences. (F) O<sub>2</sub> gradient (left) inside the microbioreactor (down right) structure and the O<sub>2</sub> barrier and sensing pillars with O<sub>2</sub>-sensing microbeads (pink circles) (right). Reproduced with permission [45], copyright 2017, Springer Nature.

### 2.1.2. Microparticle-Based Sensors

Micro-sized materials such as microbeads and microspheres loaded with luminescent dyes have also been used in luminescent O<sub>2</sub> sensing inside chip. This method benefits from simplicity of optical O<sub>2</sub> detection and add up the advantages of microparticles such as higher surface area with higher interactive surface which enhance the sensitivity, protecting the dye from decay and also lower analyte diffusion distances that enable them to have a faster response. [17,41,67,69,70]. These microparticles are mostly made of polymers such as microparticles of polystyrene (PS), poly (dimethylsiloxane) (PDMS) and silica [65,70]. they have lower analyte diffusion distances that enable them to have a faster response [17,41,67,69,70].

Jiang et al. described a microfluidic-based method to make monodisperse PDMS microbeads containing PtTFPP dye for O<sub>2</sub> sensing. After microbead characterization (150 µm diameter), they tested the efficiency of the O<sub>2</sub> sensors by spreading them over the bottom of the microfluidic channel of the PMMA chip and exposing them to pure nitrogen (0% O<sub>2</sub>) and air (21% O<sub>2</sub>) flow. Similar to the conventional film layers, the phosphorescence effects of the microbeads were quenched by an increase in their O<sub>2</sub> content (shown in Figure 1D) [68]. Their higher gas permeability, chemical inertness, nontoxicity, and biocompatibility have made them a more interesting choice for this application. In a relatively similar strategy, PS microbeads (3 µm diameter) with PtTPTBPF dyes were used for the 2D and 3D hydrogel-based cell culture chips which had a sensor spot to connect to a fiber optic and portable commercial FireStingO2 optical O<sub>2</sub> m (Pyroscience, Aachen, Germany) [17].

A novel liver-on-chip with O<sub>2</sub> monitoring has used tissue-embedded PS microparticles (50 µm diameter) loaded with ruthenium-phenanthroline-based phosphorescence dyes. The system was designed for the study of mitochondrial dysfunction using an organoid of HepG2/C3A cells [69]. Figure 1E shows that each microwell was first loaded with about 100,000 cells and 20 O<sub>2</sub>-sensing beads. The figure also illustrates the whole bioreactor (a) and its organoids-containing PDMS microwells (b), as well as fluorescent imaging of the organoid incubated overnight with O<sub>2</sub>-sensitive microbeads (c). The microbeads embedded in the tissue can also be used to assess the cell's O<sub>2</sub> uptake and metabolism rate in real-time measurement. The availability of a continuous O<sub>2</sub> uptake measurement over 28 days was mainly due to the bioreactor design, in which the microbeads existed in the trapped cells and are involved in cell migration. This method also guaranteed the absence of any necrosis. The number and location of the microbeads during the experiment, therefore, were fixed over time. In another study with similar microbeads and concepts, O<sub>2</sub> monitoring was carried out in a liver-on-chip to test different drugs [47].

Another team designed a microbioreactor for recapitulating intratumor O<sub>2</sub> gradients to study the solid tumor microenvironment. The cellular metabolism and physical constraints of a cell layer (MCF-7 cells) between the two diffusion barriers were used in a tumor section-like culture method. The O<sub>2</sub> gradient was mimicked without the need for using any O<sub>2</sub>-gradient making devices [45] (Figure 1F). In order to achieve the gradient, silica microparticles were loaded with an O<sub>2</sub>-sensitive luminescent dye (tris(4,7-diphenyl-1,10-phenanthroline) ruthenium(II) dichloride), which were glued to the pillar by a PDMS layer inside the microfluidic channels. The fluorescent imaging showed a uniform signal from the O<sub>2</sub>-sensitive microbeads, which could distinguish different degrees of hypoxia in real-time and perform spatially resolved measurements superior to conventional imaging-based systems in the OOC devices [45]. In another study, microbeads were used to simultaneously detect O<sub>2</sub> and pH to study embryonic development inside a single zebrafish embryo culture system. Embryo culture microwells were composed of two sensing hydrogel (Poly(ethylene glycol) diacrylate (PEGDA)) layers. PS microspheres with Pt-porphyrin dyes were used to study the O<sub>2</sub> consumption rate (OCR) while dextran microbeads loaded with a (2',7'-bis-(2-carboxyethyl)-5-(and-6)-carboxyfluorescein (BCECF)) dye were applied for sensing the acid extrusion rate (AER). The O<sub>2</sub>-sensing system was reported to be efficient and capable of monitoring low OCRs of a single early embryo captured in a closed microwell [46].

### 2.1.3. Nano-Enabled Sensors

The application of nanoparticles (NPs), nanostructures and nanocomposites in sensors has been of great interest over the past decade. This is mainly because of wide range of source materials, shapes and surface functionalization options which increase the flexibility of choosing the suitable nanoparticle for the sensing strategy of each study. The smaller size and/or pores of such materials increase their aspect ratio as well as their active surface, thereby improving their reactivity to a greater degree compared to micro-sized materials. The presence of functionalized groups for attachment to different surfaces, linkers and molecules on their surface expands their features and applications. The unique optical and plasmonic properties of NPs has great potential for enabling rapid and sensitive O<sub>2</sub> optical sensing. Moreover, these NPs make the dyes more soluble and protect them from direct contact with the solutions which protect the dye from decay and also from potentially interfering molecules inside the chips and improve the selectivity and storage ability of the chip O<sub>2</sub> sensor [71–75]. NPs based on polymers such as poly (methyl methacrylate) (PMMA), PS, poly(styrene-block-vinylpyrrolidone), poly(styrene-co-maleic anhydride), (poly(fluorene-alt-benzothiadiazole)), are among the most commonly used types in microfluidic devices [65,70].

The application of NPs for O<sub>2</sub> sensing in cells has been studied by the synthesis of PMMA NPs loaded with Pt(II) Octaethylporphine (PtOEP) dye and surface modification with Poly L-lysine (PLL), which makes the system biocompatible and easy to enter the living cells due to their positive charges. These NPs are efficient in sensing dissolved O<sub>2</sub> (DO) concentrations as low as 0–43 ppm [71]. The NP-based O<sub>2</sub> sensing has also been applied in microfluidic chips for bacterial growth monitoring. They benefited from PS NPs with platinum (II) 5, 10, 15, 20-meso-tetraphenyltetrabenzoporphyrin (PtTPTBP) dyes for rapid and simple monitoring of the metabolic activity of bacteria for 72 h [72]. In another study, Horka and colleagues used poly(styrene-block-vinylpyrrolidone) NPs with PtTPTBPF dye to monitor the metabolic activity of the bacteria via phosphorescence lifetime-based measurement strategies for O<sub>2</sub> sensing inside a microfluidic droplet [49].

In the O<sub>2</sub> sensors developed by Lasave and colleagues, polymer NPs (about 25 to 35 nm) were physically adsorbed on the silica microparticles at the bottom of the glass chip (Figure 2A). The comparison between glass chips with and without the microparticles as the NPs bed for O<sub>2</sub> sensing showed that the chips with microparticles perform better compared to bare glass [51]. They showed that the sensors were stable with fast response and capable of using detection dyes (pH-sensitive dyes). The sensors could be used inside the microfluidic channels, even closed ones, by introducing the NPs. This method, however, is limited to glass chips (not plastic-based devices).

Magnetic NPs can also be used for chip-based O<sub>2</sub> sensing. For instance, magnetic NPs and PtTFPP dyes (luminophore dyes) were merged into the poly(styrene-co-maleic anhydride) (PSMA) polymer to form a magnetic nano-complex. They were brought together via an external magnet over the chip's sensing spot, while the imaging or optical fibers were used as the readout [51]. The sensing spots can measure not only the other O<sub>2</sub> level but also the temperature and pH.

Core-shell poly(styrene-block-vinylpyrrolidone) magnetic NPs, with a PS core and hydrophilic polyvinylpyrrolidone shell, were used for simultaneous detection of O<sub>2</sub> and pH. PtTPTBPF as an O<sub>2</sub>-sensitive dye is incorporated in the core, where the pH indicator and the reference dye are applied on the shell (Figure 2B,C) [76]. Based on the reported results, a mixture of NPs loaded with O<sub>2</sub>, and pH dyes performed better than those containing both dyes. This strategy allows simultaneous detection of the two parameters and is easy, reproducible, and stable in different circumstances. Scientists also introduced a perivascular niche-on-a-chip device, in which the intracellular levels of O<sub>2</sub> were monitored in human mesenchymal stem cells (h-MSCs) using polyfluorene NPs (poly(fluorene-alt-benzothiadiazole)) covalently conjugated with dyes (platinum(II) meso-bis(pentafluorophenyl)bis(4-bromophenyl)porphyrin (PtTFPPBr<sub>2</sub>)). They used NAD(P)H fluorescence signal as a reference in a fluorescence lifetime imaging microscopy (FLIM)

system (Figure 2D). The applied NPs are reported to have a high-intensity fluorescent signal with high cell uptake levels, resulting in the chip-based real-time assay of intracellular  $O_2$  levels. These NPs can also be easily applied to closed chips [48].

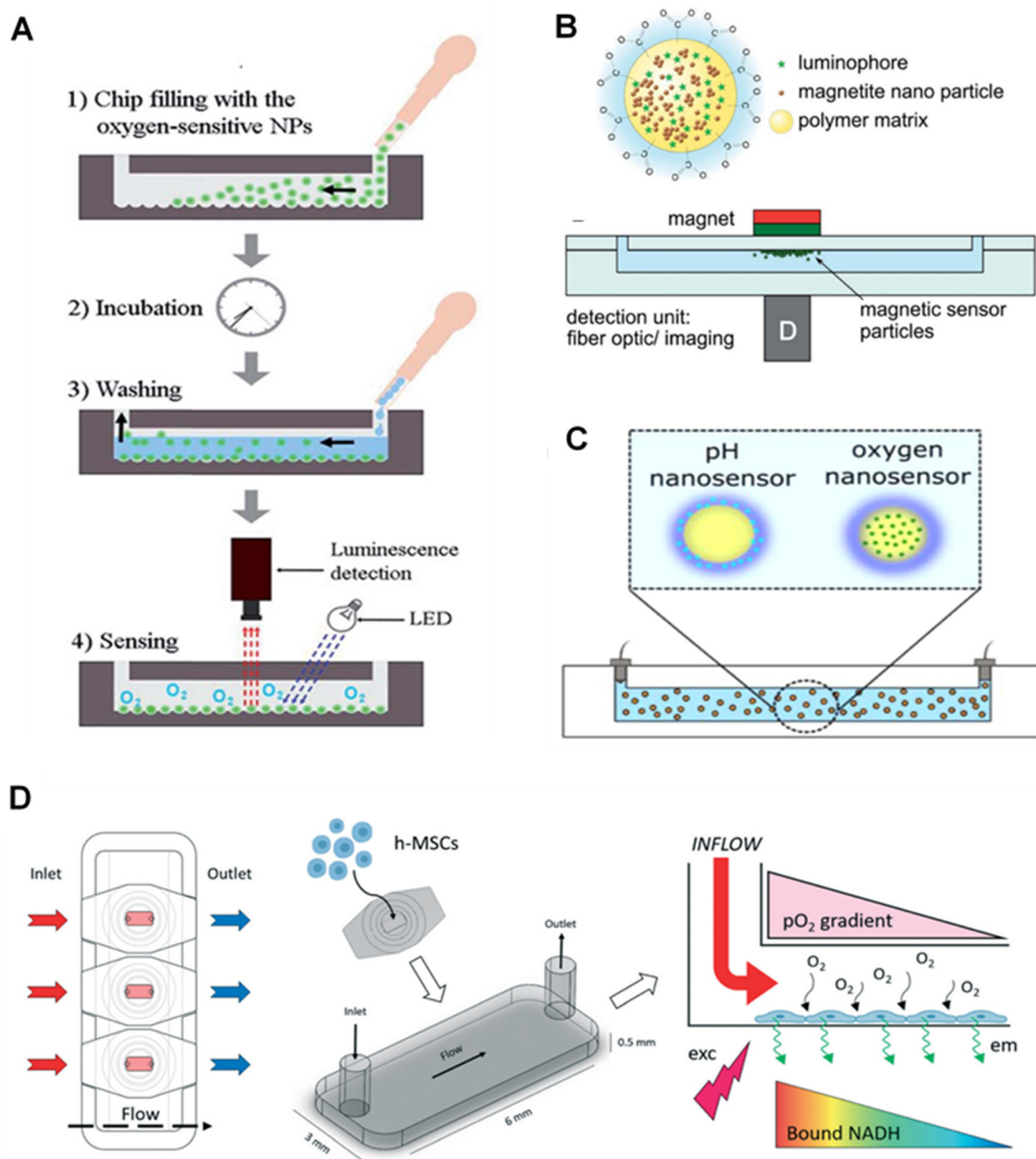


**Figure 2.** Application of nanoparticles for  $O_2$  sensors in on-chips. (A) Nanoparticles are introduced into the channels to attach to the microbeads inside the chip and form an  $O_2$ -sensitive layer. Reproduced with permission [51], copyright 2015, The Royal Society of Chemistry. (B) Magnetic NPs with luminophore come together in a spot in the chip parallel to where the outside magnet is located. Reproduced with permission [76], copyright 2014, The Royal Society of Chemistry. (C) Sensitive dyes in core-shell NPs for simultaneous detection of  $O_2$  and pH. Reproduced with permission [76], copyright 2014, The Royal Society of Chemistry. (D) Chip-based stem cell culture to monitor  $O_2$  gradient via optical luminescent sensing layers. Reproduced with permission [48], copyright 2021, The Royal Society of Chemistry.

#### 2.1.4. Commercial Probes and Portable Devices

Commercial and/or portable modules have been used for on-chip monitoring of O<sub>2</sub> levels in embryo, cell and tissue cultures [17,77]. While the benefits of portable O<sub>2</sub> sensing in microfluidic devices are well known, in OOCs, portability can bring additional features such as compactness and miniaturization of the sensing module, an automated, simple working platform with their own software, and multiplex detection of factors such as pH, CO<sub>2</sub>, and temperature besides O<sub>2</sub>. In this regard, few companies have introduced commercial portable Universal Serial Bus (USB)-based optical readout systems such as FireStingO2 (PyroScience, Aachen, Germany) [17,77], Piccolo2 device (PyroScience, Germany) [49,50] or portable detection modules such as VisiSens device (PreSens, Regensburg, Germany) [77]. These optical readout modules can be mounted on (Figure 3A) or connected to (Figure 3B) the sensing spot on channel/chamber or implemented in a modulated box (Figure 3C).

For Example, Ehgartner et al. introduced sensor spots integrated with silicon-glass microreactors connected with commercial optical readout devices [78,79]. Figure 3A represents the chip and its sensing spots (left) as well as the commercial piccolo2 readout with a USB port (right) which can be connected to the computer for further analysis. The chip was designed to measure the O<sub>2</sub> level and to monitor the enzymatic activity of D-amino acid oxidase and glucose oxidase as model enzymes. Seven cell culture chambers and four O<sub>2</sub> sensing spots were read by a simple USB O<sub>2</sub> m (Piccolo2) connected to an optic fiber or by a four-channel optical O<sub>2</sub> m (FireStingO2). The chip was compatible with two famous luminescent O<sub>2</sub>-sensitive dyes, with two for PdTPTBPF and the other two for PtTPTBPF. The method, therefore, was concluded to be accurate with an automated and inexpensive production line and compatible with commercial readout devices. In another example, but for monitoring the metabolism of bacteria in droplets, Horka et al., also used Piccolo2 device enabling the non-invasive contactless measurement through the wall of a tubing as it is shown in the Figure 3B [49].

Zhu et al. introduced a microbioreactor for monitoring metabolic activities of zebrafish embryos with a sensor foil integrated with O<sub>2</sub> monitoring using a Fluorescence Ratiometric Imaging (FRIM) system [77]. An O<sub>2</sub>-sensing foil was integrated into an embryo trapping chamber in a PMMA chip. A portable USB-embedded commercial ViviSens detector was used for fluorescent imaging. A calibration curve was plotted before the embryo culturing for chip-based O<sub>2</sub> measurements. The method was proved to provide a real-time and non-invasive measurement for the embryos. Other advantages were the possibility to use commercial O<sub>2</sub> sensing devices and software, such as a small integrating and portable detector with USB port, and the capability of measuring O<sub>2</sub> gradient.

In another development, Wang and colleagues developed a portable detector for O<sub>2</sub> detection using a PDMS chip and a PtTFPP film [79,80]. The detector (Figure 3C), comprised of a photomultiplier (PMT) counter (with a Charge Coupled Device (CCD) camera and an imaging spectrograph) connected to a smart-phone application and was able to detect DO levels with an LOD of 0.01 mg/L (0.37 µM) and short response time of 22 s. The simplicity, low-cost production, handling of the device, high sensitivity, short response time and portability are among important features which make this detector a desirable device for on-chip O<sub>2</sub> sensing, especially in medical applications.

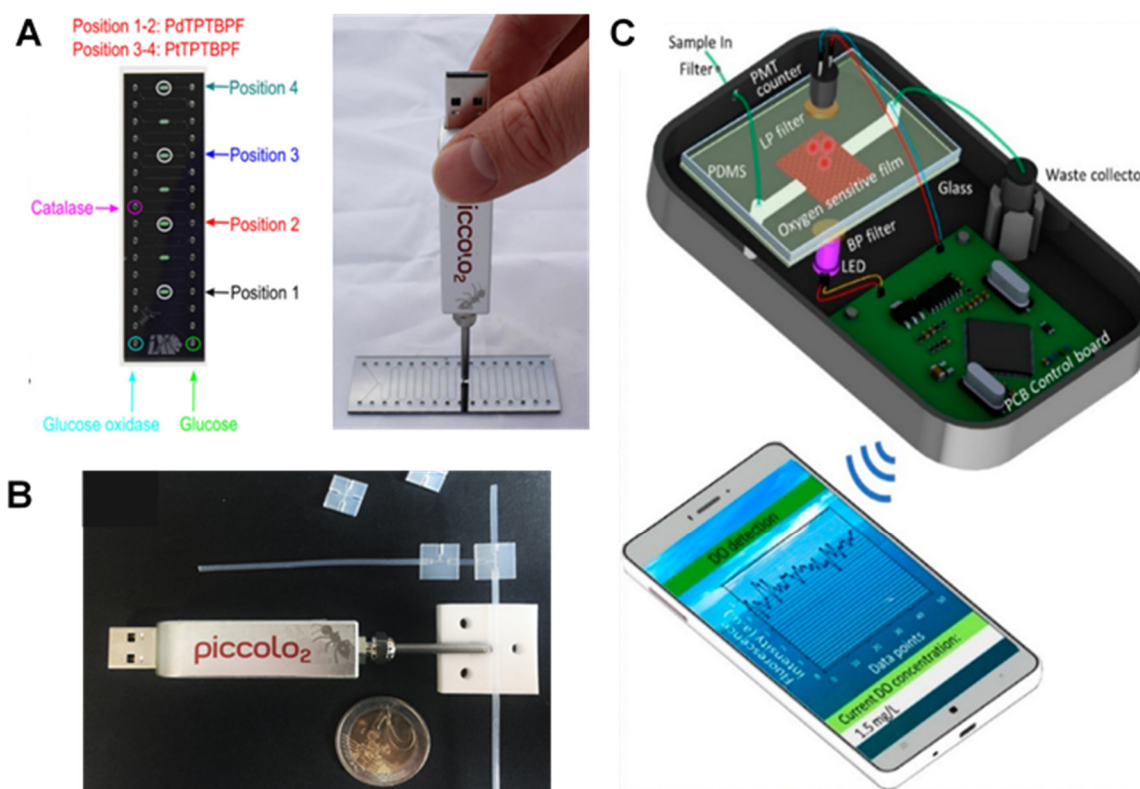


**Figure 3.** Commercial and portable optical readout systems for on-chip O<sub>2</sub> monitoring. (A) A chip (left) designed for commercial optical readout devices (right). Reproduced with permission [78], copyright 2016, Elsevier. (B) chip-based bacteria study with O<sub>2</sub> measurement through the wall of tubing using a commercial readout device. Reproduced with permission [49], copyright 2016, American Chemical Society. (C) A portable handheld photodetector device connected to a mobile app for chip-based O<sub>2</sub> monitoring. Reproduced with permission [80], copyright 2021, MDPI.

## 2.2. Electrochemical Methods

Electrochemical (EC) sensing is a common technique to measure low concentrations of DO, often in microfluidic applications, with high sensitivity [81,82]. Being introduced over two decades ago, it is believed that certain shortcomings of optical measurement techniques are resolved by using EC sensing, such as the need for time-lapse bright field and fluorescence microscopy in combination with various staining techniques as well as a collection of supernatants and cellular samples traditionally used in the OCCs. However, the direct integration of EC-based DO sensors in OOC systems is not common because of the complexity, multi-step and high-temperature fabrication process and risk of material incompatibility, all of which increase the complexity of the whole system as well as the overall probability of failure [12]. In the following subsections, we review several innovations to overcome such difficulties in EC sensors and categorized into five main innovation groups: (i) novel configurations in Clark-type sensors; (ii) novel materials (e.g., polymers, O<sub>2</sub> scavenging and passivation materials); (iii) nano-enabled electrochemical sensors; (iv) novel designs and fabrication techniques; and (v) commercial and portable electrochemical readouts. Table 3 summarizes the components, advantages and LOD of the selected EC sensors for the measurement of DO.

**Table 3.** Characteristics of chip-based electrochemical O<sub>2</sub> sensors.

EC-Based O <sub>2</sub> Sensor	LOD	Advantages	References
PDMS-container structure, and the glass substrate	105 cells/mL	Short response time (6.9 s)	[83]
Low-temperature co-fired ceramic (LTCC) in an improved Clark-type DO sensor	Up to 8.1 mg/L	easy fabrication, flexible configuration, short response time (10.9 s), real-time detection	[84]
pHEMA hydrogel layer with electrolyte and PDMS as gas-permeable membrane	0.121 $\mu\text{A cm}^{-2} \mu\text{M}^{-1}$	zero analyte consumption, 1-point calibration, long-term stability	[85]
PPy as the internal contact layer between polymeric sensitive membrane and gold	$0.11 \pm 0.02 \text{ mg L}^{-1}$	Low cost, good performance and long-term potential stability	[86]
Multi-sensor glass-chip with a PDMS imprinted microfluidic channel grid	100 pA per each 1% O <sub>2</sub>	Transparent for microscopic observation, cheap, high sensitivity	[87]
Biocompatible glass chip fabricated using a hybrid thin film and laminate technologies	$0.735 \mu\text{A} \mu\text{M}^{-1} \text{ cm}^{-2}$	Low O <sub>2</sub> consumption on the electrode, long-term stability	[88]
Biocompatible PDMS biochip with Au/Nafion electrodes	50 mmol L <sup>-1</sup>	real-time and continuous O <sub>2</sub> monitoring in dynamic flow conditions	[89]
Kapton tape with embedded spirally rolled Microchannels	$12.89 \text{ nA mmHg}^{-1}$	O <sub>2</sub> and temperature sensors, embedded spirally rolled microchannels	[90]
ElecCell technological platform using PVD	6 pA/s	low-cost, easy to use and reproducible portable chip	[91]
ultra-microelectrode array (UMEA)	$0.49 \text{ nAs}^{-0.5} / \text{mg/L}$	Ultra-short response time (<5 ms), 10 times lower O <sub>2</sub> consumption	[92]
Multi-planar SPE sensor coupled with cultivation cell wells	3 mg/L	Continuous long-term O <sub>2</sub> measurement, sensor reutilization	[93]
Inkjet printing (IJP) DO sensors on the delicate porous substrate	$28 \pm 1 \text{ nA L mg}^{-1}$	low O <sub>2</sub> consumption on electrodes, short response time (60 s)	[94]
Electrochemical microsensors combined with spheroid technology	NM	fast, precise, and continuous long-term measurement of metabolic directly in the microwell	[95]
Spheroid on chip	NM	Real-time monitoring of metabolic activity and automated assays for toxicity evaluation	[96]

NM: not mentioned.

### 2.2.1. Novel Configurations in Clark-Type Sensors

The Clark-type configuration has transcended the main limitations of the optical sensors, such as high cost and complicated fabrication process. The system normally consists of an electrode covered with a thin layer of electrolyte solution and a thin polymer membrane enabling selective permeation of O<sub>2</sub> to the immersed electrode. The membrane also separates the electrolyte from the specimen, preventing cross-sensitivity and resulting in a short turnaround time. However, the need for mechanical agitation, circulation of the sample or immersion of the sensor in the sample (which requires large amounts of sample and reagents) are the main drawbacks of such sensors [81,97]. Apart from the high risk of mechanical failure in the thin gas permeable membrane, such sensors are not compatible with continuous monitoring, automation and high-throughput measurements [98].

Reducing the size of the sensor and/or limiting the measurement time is necessary to reduce O<sub>2</sub> consumption by the EC sensor and to prevent possible endangerment of the biological sample. This is important for the measurement of the kinetics of O<sub>2</sub> variation in samples and for monitoring the cell growth. Therefore, using a micro total analysis system ( $\mu\text{TAS}$ ) has overcome some of these challenges. O<sub>2</sub>-plasma bonding was one of the first methods used in miniaturized Clark O<sub>2</sub> sensors [83]. Unlike the field-assisted bonding technique, which requires high electric voltage (kV) and temperature (250 °C) to combine the glass and silicon substrates, this simple and low-temperature fabrication process enabled the integration of several semiconductor elements and polymer-material structures in an ordinary laboratory environment [99]. The use of thick-film technology

with the SU8 photoresist and extremely thin O<sub>2</sub> separation membrane resulted in a low response time (6.8 s). However, the sensor was not suitable for long-term measurements.

In a more recent attempt, a low temperature co-fired ceramic (LTCC)-based microfluidic Clark-type O<sub>2</sub> sensor was used for real-time monitoring of localized DO [84]. The advantages outlined for the LTCC materials include hermeticity and mechanical durability, high scalable prototyping/manufacturing, and the ability to directly integrate both electronic and microfluidic with a compact 3D package [100–102]. The EC sensor consisted of a solid proton conductive electrolyte that facilitated the fabrication process and improved shelf life. The solid-state proton conductive matrix (PCM) membrane (Nafion 117 membrane) was used as a support to lower the risk of mechanical failure of the PDMS O<sub>2</sub> permeable membrane (OPM). Also, the microfabricated electrodes and continuous flow of the sample through the microchannel could reduce the O<sub>2</sub> depletion risk.

Clark-type O<sub>2</sub> microsensors also promise zero analyte consumption if the feedback mode (Ross principle) is successfully implemented [103]. According to this principle, a suitable sensor configuration allows for the compensation of O<sub>2</sub> consumption at the working electrode (WE) through evolving O<sub>2</sub> at the counter electrode (CE) while maintaining the sensor pH. This is confirmed by showing O<sub>2</sub> formation as the only oxidation reaction at the CE. Another example is a microsensor with Pt as WE was fabricated on a glass chip using thin film technology. The use of a poly-2-hydroxyethyl methacrylate (pHEMA) hydrogel layer containing buffer solution as an electrolyte and PDMS as a gas-permeable membrane showed promising results in monitoring cell respiration in cultures (Figure 4A) [85]. Thanks to the dried-out hydrogel layer, the microsensors could be stored dry and activated by immersion into aqueous analytes. As a result, the measurement in the gas atmosphere, even with ambient humidity, was possible only for less than one hour. Chronoamperometric protocols to renew the electrode surface through the formation of PtO and subsequent removal before O<sub>2</sub> measurement was applied to enable long-term stability, for more than one week, without any need for recalibration.

In order to simplify and speed up the prototyping process, a confined microfluidic cell culture system was developed using a microscopic indium tin oxide (ITO) slide with planar Pt sensors at the bottom of a plate for the measurement of acidification, O<sub>2</sub> consumption, and cell adhesion [104]. The structure of the slide, along with the gas permeability of the PDMS lid, ensured 100% air saturation in the culture medium, desirable for the cells but responsible for possible bubble formation. Using an ultrashort pulse laser, the fabrication process of such amperometric Clark O<sub>2</sub> sensors took about three minutes per chip. This not only improved the precision of the chip but also prevented possible exposure to toxic chemicals or adverse effects in the cell culture.

In a clinical application of a multi-analyte OOC, dynamic measurement of DO was performed in low volumes of urine using Clark-type microsensors with a high sensitivity of  $3.60 \pm 0.2 \text{ nA mg L}^{-1}$  [86]. The multi-sensor platform was composed of three different polymeric layers: a 127 mm thick polyimide film (Kapton<sup>®</sup> 500HN, DuPont Co., Wilmington, DE, USA incorporating the gold microelectrode array, a 175 mm structured Polyethylene terephthalate (PET)-two-side adhesive sheet (AR8939) defining the microfluidic manifold, and a 188 mm cyclo-olefin polymer (COP) film (Zeonex ZF14-188, purchased from Ibsi, Gräfelfing, Germany) as the cover. The use of flexible polyimide Kapton<sup>®</sup>, besides its thermal and mechanical stability, high chemical resistance, and low dielectric constants, ensured the platform was cost beneficial.

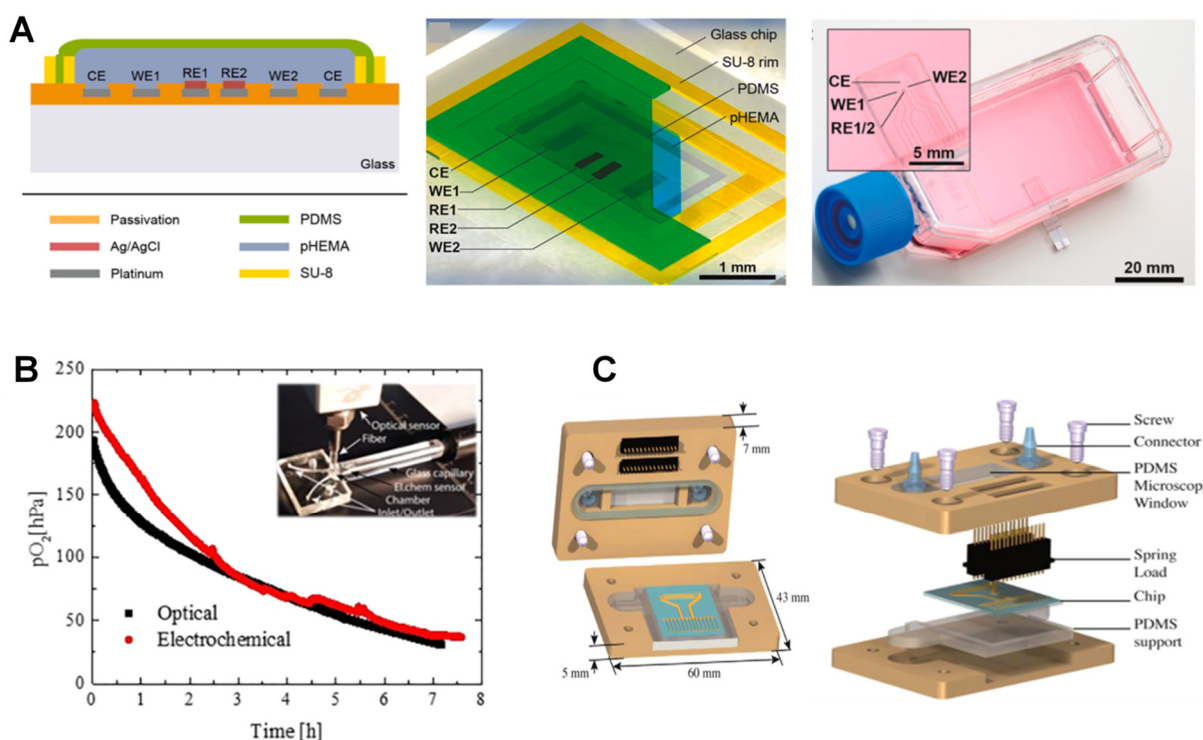


**Figure 4.** Electrochemical sensors for on-chip O<sub>2</sub> measurement. (A) cross-section and top view of the Clark-type O<sub>2</sub> monitoring microsensor via chronoamperometric sensing protocols in cell culture and organ-on-chip systems. Reproduced with permission [85], copyright 2020, Elsevier. (B) microfluidic cell culture chip with intra-channel parallel electrochemical and optical O<sub>2</sub> measurement using commercial optical and electrochemical readout devices showing agreement between the results (red and black curves). Reproduced with permission [105], copyright 2019, American Chemical Society. (C) Components and cross-section of the microfluidic chip with electrochemical detection electrode arrays for a distinct set of three-electrode for O<sub>2</sub> and the electrode array for Na<sup>+</sup>, K<sup>+</sup> and pH measurement. Reproduced with permission [106], copyright 2015, Elsevier.

### 2.2.2. Novel Materials: Polymers, O<sub>2</sub> Scavenging and Passivation Materials

As mentioned in the previous section, polymer membranes are an important part of EC-based O<sub>2</sub> sensors. This is because O<sub>2</sub> is diffused to the reaction chamber, where it is consumed, while biological cells and other organics are prevented from passing through. PDMS is the most common polymer used to construct the microfluidic channels and the sensor support because of its characteristics, such as biocompatibility, gas permeability, mechanical flexibility, and optical transparency.

In an integrated microelectrochemical reactor, an EC sensor with incorporated Pt interdigitated array (IDA) as WE, a Pt CE, and Ag pseudo-reference electrodes (RE) were used. The WE was fully immersed in a liquid electrolyte confined in the channels [107]. The O<sub>2</sub> reduction reaction (ORR) was used in this platform for both pH tuning and fluid actuating reactions. In this regard, a microelectrochemical cell design inherent to membrane-covered Clark-type sensors was used. Unlike common polymers that are less permeable to O<sub>2</sub> than the electrolyte, a highly permeable PDMS membrane, capable of supporting significant current densities, was used. This simple change enabled remarkable pH gradients capable of initiating and/or sustaining marked fluid displacements within the microfluidic channel system with low applied potentials (0.1 V) and no need for additional electrochemically active components. Due to the high O<sub>2</sub> permeability of PDMS, the microfluidic cell supported significantly higher current densities in the ORR compared to those measured in conventional (quiescent) EC cells with similar electrode areas. This results in achieving more stable ORR currents. Another advantage of this system is the absence of bubbles. Using membranes thinner than 0.1 mm allows for a higher diffusion rate with limited ORR

current densities. The significant O<sub>2</sub> mass transfer in the PDMS structures of the microfluidic cell helped generate transient chronoamperometric waveforms while sustaining the steady-state mass transfer limited the ORR current densities.

As another example, a multi-sensor glass chip with a PDMS imprinted microfluidic channel grid was developed to characterize cellular behavior [87]. The microfluidic manifold was fabricated based on the Haversian bone-canal system to ensure a homogeneous flow. They resembled a Clark-type amperometric sensor without any O<sub>2</sub>-selective membrane. The glass-wafer technology ensured the microscopic observability of the on-chip cell culture along with online monitoring of the physiological parameters. On the other hand, glass is less costly compared with silicon-sensor technology [88,108–110]. Circular 78.5 μm<sup>2</sup> Pt electrodes, as O<sub>2</sub> sensors, led to a sensitivity of 100 pA per each 1% increase in saturated air (21% O<sub>2</sub>). The sensor worked for 80h during cell culture, and the fluctuations noted in the current rates were possibly due to large gas bubble formations.

Although PDMS is the most common polymer used in this regard, other polymers have also been tested. PTFE has higher permeability and faster O<sub>2</sub> diffusion rates compared to PDMS, which results in O<sub>2</sub> depletion in the channel [111]. Adjusting the electrolyte flow rate and the channel length can ensure the presence of sufficient O<sub>2</sub> in the biomass chamber and thus the reliability of the results. However, PDMS-based respirometers allow shorter analysis times, especially when thicker membranes are needed or the sample is rich in organic matter. Using gas permeable membranes such as PDMS alone has limitations such as loss of vapor which changes the fluid composition of the microfluidic cultivation chambers and may lead to reoxygenation from the ambient air. Other materials benefit from diffusion and mixing deoxygenated fluids, chemicals, electrolytic, photocatalytic, and biological O<sub>2</sub> depleting liquids such as sodium sulphite and pyrogallol [112]. These materials, however, can interfere with the cellular processes and metabolic pathways. Using an external gas supply with nitrogen to equilibrate the O<sub>2</sub> concentrations is another alternative, even though it is less accurate [113].

Functional microfluidic materials with intrinsic O<sub>2</sub> scavenging properties allow for long-term cell cultivation under reduced O<sub>2</sub> concentrations. These are cheap substitutes for bulky and expensive hypoxic chambers. Adjusting the temperature and curing time during the process of fabrication and altering the microfluidic layout and the surface area-to-volume aspect ratios of the channels, as well as modifying the flow rates during cell cultivation, can help fine-tune the O<sub>2</sub> scavenging rates and address specific biological issues. In an example of a miniaturized OOC with embedded O<sub>2</sub> sensors, an off-stoichiometric thiol-one epoxy polymer was integrated into a functional biochip to efficiently remove DO to below 1.0 hPa. In a clinical application, this system was used to study acute ischemic stroke using a murine blood–brain barrier (BBB) model (Figure 4B) [105]. In this system, anaerobe bacteria were cultivated under ambient air until efficient germination of pathogens was achieved. They compared two parallel O<sub>2</sub>-sensing methods: an opto-chemical O<sub>2</sub>-sensing based on luminescence lifetime measurement using an O<sub>2</sub> indicator luminescent dye (PtTPTBPF) and an EC sensor directly detecting DO levels by oxidation at the electrode surface measured by a commercial readout OX-NP Clark-type sensor (Unisense, Denmark). Both sensors had similar time-dependent O<sub>2</sub> depletion profiles, resulting in O<sub>2</sub> tension of 30.76 and 37.58 hPa after 7 h, respectively. They showed similar DO removal from about 200 to 30 hPa within 7 h in a 25 μL microchannel volume. O<sub>2</sub>-sensitive microbeads, however, were selected as the best options because of their smaller footprint and ease of integration within the microchannels.

Passivation materials are also used to not only define the electrode surface but also ensure their long-term EC stability. In an attempt to develop a low-cost, easy-to-use, reproducible and portable microfluidic device, a specific B33 glass substrate was used [91]. The idea was to initiate and monitor microalgae photosynthesis activity while electrochemically assessing the microalgal O<sub>2</sub> production rate during artificial night/day cycles. The ElecCell (Electrochemical microcell) technological platform, with fully integrated EC microcells (titanium/platinum (Ti/Pt) as the working microelectrode, the counter and the sub-structure

of the pseudo-reference) was developed using double physical vapor deposition (PVD). A silicon nitride ( $\text{SiN}_x$ ) wafer-level was deposited for passivation using low-temperature PVD. The microfluidic system was fabricated through laminating dry films to overcome the need for any micropumps or other fluid actuation devices.

In another scalable microfluidic platform developed for continuous monitoring of biofilm proliferation and activity under shear stress conditions, a double layer of PVD deposited silicon oxide and silicon nitride ( $\text{Si}_3\text{N}_4$ ) was applied for passivation purposes (Figure 4C) [106]. The combination of two interdigitated microelectrodes (IDuEs) and punctual electrodes helped with the measurement of DO,  $\text{K}^+$ ,  $\text{Na}^+$  and pH. The optimized IDuEs permitted sensitive and reliable label-free monitoring of *Staphylococcus aureus* V329 growth. The four-electrode system eliminated possible electrode-electrolyte effects, improving sensitivity and providing morphological and structural information necessary for assessing the bacterial growth on the electrode. A combination of polycarbonate and PDMS was used to fabricate the upper and lower lids, respectively. The novel platform could thus be integrated into multiple environments, allowing simultaneous optical microscopy and impedance spectroscopy measurements.

### 2.2.3. Nano-Enabled Electrochemical Sensors

Nano-enabled sensors are those types use nanomaterials or nanolayers of materials in order to enhance the sensitivity of the oxygen measurement and electrical and mechanical properties of the used materials. Nafion is a permeable membrane that enhances the electrodes' shelf life and their sensitivity due to its anti-fouling properties. In an example of miniaturized cell-based biochips for toxicological analysis during cell growth and development, EC amperometric sensors were integrated at the inlet and outlet microchannels of a PDMS cell chamber to perform real-time continuous glucose and  $\text{O}_2$  monitoring [89]. Two arrays of thin-film gold microelectrodes ( $0.16$  and  $0.016$   $\text{mm}^2$  for glucose and  $\text{O}_2$ , respectively) were incorporated in a biocompatible PDMS microfluidic cell culture device. Nafion-modified  $\text{O}_2$  sensors could measure  $\text{O}_2$  concentrations from 237 to 50  $\text{mmol L}^{-1}$  with a sensitivity of  $0.50 \pm 0.05$   $\text{nA mol}^{-1}\text{O}_2 \text{ L}^{-1}$ . The integrated Au/Nafion electrodes were concluded to be suitable for DO monitoring in dynamic flow conditions with high stability and short response time. The flow rate, however, needed to be controlled due to the high  $\text{O}_2$  permeation through the PDMS.

A lab-on-a-tube (LoT) integrated with spirally-rolled pressure, temperature,  $\text{O}_2$  and glucose microsensors was developed for multimodal real-time neuromonitoring as well as draining CSF in patients with traumatic brain injury [90]. The approach was reported to be less invasive and cheaper compared with traditional techniques. The temperature and DO sensors helped adjust the output, reducing errors commonly seen in in-vivo biosensors. DO sensors, the focus of the current review were fabricated on 25 mm thick Kapton film patterned with Ti/Ir/Au and finally parylene layers. The Au layer on the reference electrode was selectively etched, and iridium oxide ( $\text{IrO}_x$ ), a promising material for in-vivo reference electrodes, was grown anodically in a 0.7 M  $\text{Na}_2\text{HPO}_4$  solution. Nafion and silicone membranes were deposited as a polymer electrolyte and  $\text{O}_2$  permeable layer, respectively. With a sensitivity of  $12.89$   $\text{nA mmHg}^{-1}$ , DO sensors could continuously monitor percentage of  $\text{O}_2$  of 152 mmHg (air-saturated) and 38 mmHg (5%  $\text{O}_2$ ) for at least five days with less than 9% sensitivity error.

### 2.2.4. Novel Designs and Fabrication Techniques

The use of an ultra-microelectrode array (UMEA) for ultra-short (<5 ms) measurements is another novel technique to monitor DO concentrations in any solution [92]. As an example, the sensor consisted of Pt electrodes recessed in a glass substrate with oxide-nitride-oxide (ONO) as the insulating material. Such sensor was reported to have a high sensitivity of  $0.49$   $\text{nAs}-0.5/\text{mg/L}$  with a drastically (about 10 times) low OCR, valuable for in situ assessment of the microtissues' respiratory activity. One of the main limiting factors for the lifetime application of such sensors is the need for repeated recalibration.

This drawback has been addressed by arranging the cell cultures and sensors in a multi-well system in a way that they come in contact with each other at certain times and then separated at others such that the measurement would have no impact on the cell growth [93]. The bottom side of the cultivation wells, made of 0.1–0.3 mm thick Al<sub>2</sub>O<sub>3</sub> membrane with interconnecting pores (200–300 nm), was connected to the sensor area using a special coupling mechanism. The planar multi-sensor chip was made of screen-printed electrodes (SPEs) on the Al<sub>2</sub>O<sub>3</sub> substrate, with those dedicated to O<sub>2</sub> measurement covered with pHEMA and PUR membranes using dispensing technology. The gap between the two modules enabled the repeated flow of the analyte-containing liquid through a biocompatible nano-porous sterile membrane, resulting in continuous pH, glucose and O<sub>2</sub> measurement during the cultivation phase. The system could be reutilized after sterilization with gamma-rays.

Inkjet printing (IJP) is a novel technique used for sensor fabrication. The main advantage of this technique is its compatibility with delicate substrates that cannot withstand high temperatures due to the possibility of drop-on-demand material deposition. Moreover, the direct writing approach without masks reduces the overall cost and fabrication time considerably and facilitates iterative design changes. Multiple sensors are integrated into an extremely thin, porous, and delicate membrane inside the OOC in such applications. The DO sensors are printed along the microfluidic channel allowing local online monitoring of O<sub>2</sub> concentrations. A primer biocompatible dielectric layer (SU-8) is commonly used to seal the porosity of the membrane at defined areas, build a uniform deposition of conductive inks, accurate definition of the electrode area, and prevent possible short circuits [114]. In one example, DO sensors were fabricated using IJP in ExoLiver, a liver-on-a-chip device for real-time monitoring of the cell culture, O<sub>2</sub> gradient, and OCR [94]. ExoLiver, a modular bioreactor consisting of two plates separated by a porous membrane, mimics the liver sinusoid system. The 300 µm DO sensors had a negligible O<sub>2</sub> consumption of about  $2.94 \times 10^{-8} \text{ mg s}^{-1}$  per sensor, therefore not affecting the viability of the cell culture. They were calibrated by polarization at −650 mV, an optimal reduction potential value for determining DO concentrations without interfering with the electro-active medium. The sensor had a sensitivity of  $28 \pm 1 \text{ nA L mg}^{-1}$  (range, 0–9 mg L<sup>−1</sup>) with a turnaround time of the 60s. A max of 17.5% gradient measured between the system inflow and the outflow could be due to the metabolic activity of the sinusoidal hepatocytes and cell consumption along with the bioreactor's lower plate. This is of great value as the O<sub>2</sub> gradient has a critical regulatory role, as it is directly linked with the metabolic zonation, morphology and xenobiotic transformation in the hepatocytes.

In another clinical application, the multi-analyte microphysiometer (MAMP), a modified Cytosensor Microphysiometer combined with additional amperometric glucose, lactate, and O<sub>2</sub> sensors, enabled real-time measurement of changes caused by the metabolism of cells immobilized in a microfluidic chamber [115]. The unique combination allowed for the monitoring of both aerobic and anaerobic respiration. The main benefits of the planar SPEs include simple fabrication, versatility, high reproducibility, and low cost, all resulting in a simplified microfluidic chamber. A Dimatix materials inkjet printer was used to deposit the enzyme and polymer films on Pt SPEs to fabricate the glucose, lactate, and O<sub>2</sub> sensors. This process guaranteed the homogenous coating of the electrode surface and its reproducibility. Low concentrations of BSA-PB solution instead of BSA also reduced the risk of bubble formation. A newer generation of MAMP was later developed consisting of five modifiable Pt electrodes along with an Ag/AgCl quasi-reference, designed to measure glucose, lactate, O<sub>2</sub>, and pH simultaneously in a single microfluidic channel [116]. Reproducible surface modification was again performed using IJP. The O<sub>2</sub> sensor was modified with 2.5% Nafion. The highly adaptable system could act as a microphysiometry platform with a lifetime of up to 6 weeks.

Optical transparency of the OOC chip is obligatory for ongoing monitoring of cells using phase-contrast microscopy. This is while most of the existing microphysiometers, i.e., the Cytosensor<sup>®</sup> and Bionas Discovery<sup>™</sup> 2500 system, are silicon chips [117,118]. To

overcome these shortcomings, an optically transparent multi-parametric microphysiometer was developed for continuous dynamic measurement of pH, O<sub>2</sub>, lactate and glucose in T98G human tumor cell cultures [88]. The biocompatible glass-based chip was composed of EC microsensors fabricated using a hybrid thin film and laminate technology. Microfluidics enabled controlled medium exchange and substance exposure to low volumes (<10 µL) with low flow rates (2 µL/min), reducing shear stress on the cells. The sensors were located upstream in the inlet channel (control), inside the cell cultivation area and downstream in the outlet channel. In order to separate the biosensors from the cell culture area, protect the cells from hydrogen peroxide exposure and prevent O<sub>2</sub> depletion during cultivation, the fluidic channels and electrodes were fabricated using a permanent epoxy resist and were partly covered with a laminated polyimide film. The amperometric reduction of DO at the thin-film Pt-based circular electrodes of the O<sub>2</sub> sensors resulted in a sensitivity of  $-0.735 \mu\text{A } \mu\text{M}^{-1} \text{cm}^{-2}$  ( $\pm 0.013$ ). The sensor, however, showed a 10% decrease in sensitivity when first entered into the cell culture medium, possibly due to protein adsorption on the electrode. The O<sub>2</sub> sensors were reportedly stable for the long-term with linear behavior and negligible O<sub>2</sub> consumption (<3%).

#### 2.2.5. Commercial and Portable Electrochemical Readouts

Commercial products have been used in EC methods for the measurement of O<sub>2</sub> inside the chips. For example, the liver-on-a-chip device developed by Moya and colleagues in 2018 [94] and the blood–brain barrier (BBB) model developed by Sticker and colleagues in 2019 [105] have used the OX-NP Clark-type commercial EC readout device by Unisense Co., Denmark. A modular portable method was developed for cell culture monitoring [93]. The Bionas Analysis System 2500 (Bionas GmbH, Warnemünde, Germany, [www.bionas.de](http://www.bionas.de), accessed on 20 October 2021) was used for in-vitro, non-invasive and parallel measurement of metabolic parameters of respiration, acidification and cell adhesion in time-frames ranging from minutes to days [119]. The Clark-type sensors detected O<sub>2</sub> mediated current (charge transfer rate) with a sensitivity of  $0.12 \text{ pA} \cdot \text{s}^{-1} \pm 0.21$ . The use of the Koester coating protocol helped ensure comparable conditions for cell growth on different surfaces [120]. The inhomogeneity in cell distribution and growth over the entire chip surface, in practice, resulted in variations in values measured by the same sensors of the chip.

Another miniaturized EC respirometer monitored DO concentrations in water samples semi-continuously, unlike traditional expensive biochemical O<sub>2</sub> demand (BOD) methods [121]. The device was composed of a double-flow cell, reaction chamber, housing the sample and microbial mixture, and an electrolyte chamber, separated by a thin membrane from the bioreactor to provide sufficient flexibility to perform measurements in a wide range of organic matter concentrations. In another attempt, a novel encapsulation design and a membrane barrier material, the Intelligent Mobile Lab for In-Vitro Diagnostics (IMOLA-IVD), was used for cellular microphysiometry [96]. Extracellular acidification (EAR) and O<sub>2</sub> uptake (OUR) rates were passively monitored using a modular, label-free EC platform. A three-electrode membrane-free Clark cell was used to measure the DO levels. Above and under the 3D multicellular spheroids, the integrated layers allowed fluidic contact between the spheroids in microwells and the BioChip sensors while preventing any washout from medium perfusion.

The 3D cellular models mimicked the native environment of the tissue; however, their increased size and geometry, as well as limited access to O<sub>2</sub> and nutrients due to restricted diffusion into the scaffolds, were the main limiting factors [122]. Multicellular spheroids incorporated with OOC platforms are a promising solution. EC microsensors with a small cross-section can be inserted directly into a microtiter plate well containing a single spheroid, microtissue or organoid. Due to their high sensitivity, excellent selectivity and defined zero-point, such EC sensors can measure small changes in O<sub>2</sub> concentrations in the microtiter plate caused by the spheroid metabolism [95].

### 3. Conclusions and Future Perspectives

In this review, we discussed recent advancements of oxygen sensors in on-chip systems and categorized them in two main groups: optical and electrochemical methods. We also discussed recent research and novelties in each section with schematic Figures and an overview Tables. The optical methods are reported to be more sensitive, easier to operate and cheaper compared to the EC methods. In most cases, they do not consume O<sub>2</sub> during the process. In addition, they are compatible with commercially available luminescent dyes and optical readout devices, even fluorescent microscope which is convenient and available in most cell and tissue process centers. These sensors can be used for contactless monitoring by adding a sensing spot outside the chip readout or optical fiber, making the handling and sterilizing of the chip simpler. In addition, they do not need recalibration or experience decay over time. Compared with EC methods, therefore, these techniques are more commonly used in OOC applications. This is especially important for low concentrations of the sample when the stability and reusability of the sensor and its remaining intact are crucial. On the other hand, the EC methods have a shorter response time, and in most cases, a higher sensitivity than the previous group. In most cases, they can be used as label-free sensors, which again reduces the cost of sensor fabrication compared with optical ones. However, their integration in the chip is relatively expensive, complicated, and sometimes requires special relatively expensive instruments (Potentiostat/Galvanostat) and skilled operators.

In the future, the use of novel materials, fabrication techniques, and chemical/physical surface modifications can help facilitate the fabrication steps, reducing the price and required specialty, making the chip-integrated O<sub>2</sub> sensors more affordable. Although there are few examples of micro- and nanomaterials used for the chip-based O<sub>2</sub> sensors of either type, the field is rapidly progressing. It is expected that a variety of materials with various properties to help with O<sub>2</sub> sensing will be used for these sensors in the near future to improve their sensitivity. This is mainly because these materials are believed to increase the active surface area, enhance the stability of the surface and increase the glow of the dyes. For instance, graphene and quantum dots can be considered as potential materials due to their exceptional optical and electrochemical properties. Micro- and nanostructures of novel metal oxides are other examples of such materials because of their catalytic activity. In addition, quantum dots (QDs) are photostable and their excitement spectra are broad, while their emission spectra are size-tunable, which makes them suitable for optical sensors. Further, using a smartphone to quantify the emitted signal can significantly simplify the measurement process. Artificial intelligence and innovations in image and signal processing help enhance the sensitivity and specificity of O<sub>2</sub> sensors. Additionally, using 3D printing to manufacture the sensors can result in flexible, rapid and low-cost designs and integration of sensors in OOCs, and improve the sensitivity of the O<sub>2</sub> sensors inside the chips. Three-dimensional printing techniques can also be used to build customizable optical holders and modules that can be integrated with mobile phones or other portable detectors.

**Author Contributions:** M.A. (Mostafa Azimzadeh), P.K., M.A. (Meitham Amereh) and N.T.; writing—original draft preparation, M.A. (Mohsen Akbari) and M.H.; editing and supervision. All authors have read and agreed to the published version of the manuscript.

**Funding:** We would like to acknowledge the support received by the National Sciences and Engineering Research Council of Canada (NSERC).

**Institutional Review Board Statement:** Not applicable.

**Informed Consent Statement:** Not applicable.

**Data Availability Statement:** Not applicable.

**Conflicts of Interest:** The authors declare no conflict of interest.

## References

1. Akram, M. Mini-review on Glycolysis and Cancer. *J. Cancer Educ.* **2013**, *28*, 454–457. [[CrossRef](#)] [[PubMed](#)]
2. Bonora, M.; Patergnani, S.; Rimessi, A.; De Marchi, E.; Suski, J.M.; Bononi, A.; Giorgi, C.; Marchi, S.; Missiroli, S.; Poletti, F.; et al. ATP synthesis and storage. *Purinergic Signal.* **2012**, *8*, 343–357. [[CrossRef](#)] [[PubMed](#)]
3. Bennett, N.K.; Nguyen, M.K.; Darch, M.A.; Nakaoka, H.J.; Cousineau, D.; ten Hoeve, J.; Graeber, T.G.; Schuelke, M.; Maltepe, E.; Kampmann, M.; et al. Defining the ATPome reveals cross-optimization of metabolic pathways. *Nat. Commun.* **2020**, *11*, 4319. [[CrossRef](#)]
4. Salway, J.G. *Metabolism at a Glance*; Wiley: Hoboken, NJ, USA, 2016.
5. Beckner, M.E.; Stracke, M.L.; Liotta, L.A.; Schiffmann, E. Glycolysis as primary energy source in tumor cell chemotaxis. *J. Natl. Cancer Inst.* **1990**, *82*, 1836–1840. [[CrossRef](#)]
6. Xiong, B.; Ren, K.; Shu, Y.; Chen, Y.; Shen, B.; Wu, H. Recent Developments in Microfluidics for Cell Studies. *Adv. Mater.* **2014**, *26*, 5525–5532. [[CrossRef](#)]
7. Spiller, D.G.; Wood, C.D.; Rand, D.A.; White, M.R.H. Measurement of single-cell dynamics. *Nature* **2010**, *465*, 736–745. [[CrossRef](#)]
8. McLean, I.C.; Schwerdtfeger, L.A.; Tobet, S.A.; Henry, C.S. Powering ex vivo tissue models in microfluidic systems. *Lab Chip* **2018**, *18*, 1399–1410. [[CrossRef](#)] [[PubMed](#)]
9. Oomen, P.E.; Skolimowski, M.D.; Verpoorte, E. Implementing oxygen control in chip-based cell and tissue culture systems. *Lab Chip* **2016**, *16*, 3394–3414. [[CrossRef](#)]
10. Kmiec, M.M.; Tse, D.; Mast, J.M.; Ahmad, R.; Kuppasamy, P. Implantable microchip containing oxygen-sensing paramagnetic crystals for long-term, repeated, and multisite in vivo oximetry. *Biomed. Microdevices* **2019**, *21*, 71. [[CrossRef](#)] [[PubMed](#)]
11. Moradi, V.; Akbari, M.; Wild, P. A fluorescence-based pH sensor with microfluidic mixing and fiber optic detection for wide range pH measurements. *Sens. Actuators A Phys.* **2019**, *297*, 111507. [[CrossRef](#)]
12. Ferrari, E.; Palma, C.; Vesentini, S.; Occhetta, P.; Rasponi, M. Integrating Biosensors in Organs-on-Chip Devices: A Perspective on Current Strategies to Monitor Microphysiological Systems. *Biosensors* **2020**, *10*, 110. [[CrossRef](#)]
13. Kieninger, J.; Weltin, A.; Flamm, H.; Urban, G.A. Microsensor systems for cell metabolism—From 2D culture to organ-on-chip. *Lab Chip* **2018**, *18*, 1274–1291. [[CrossRef](#)]
14. Gomez-Cruz, J.; Nair, S.; Manjarrez-Hernandez, A.; Gavilanes-Parra, S.; Ascanio, G.; Escobedo, C. Cost-effective flow-through nanohole array-based biosensing platform for the label-free detection of uropathogenic *E. coli* in real time. *Biosens. Bioelectron.* **2018**, *106*, 105–110. [[CrossRef](#)]
15. Rodoplu, D.; Chang, C.-S.; Kao, C.-Y.; Hsu, C.-H. A simple magnetic-assisted microfluidic method for rapid detection and phenotypic characterization of ultralow concentrations of bacteria. *Talanta* **2021**, *230*, 122291. [[CrossRef](#)]
16. Guo, S.; Stevens Corey, A.; Vance Tyler, D.R.; Olijve Luuk, L.C.; Graham Laurie, A.; Campbell Robert, L.; Yazdi Saeed, R.; Escobedo, C.; Bar-Dolev, M.; Yashunsky, V.; et al. Structure of a 1.5-MDa adhesin that binds its Antarctic bacterium to diatoms and ice. *Sci. Adv.* **2017**, *3*, e1701440. [[CrossRef](#)]
17. Zirath, H.; Rothbauer, M.; Spitz, S.; Bachmann, B.; Jordan, C.; Müller, B.; Ehgartner, J.; Priglinger, E.; Mühleder, S.; Redl, H.; et al. Every Breath You Take: Non-invasive Real-Time Oxygen Biosensing in Two- and Three-Dimensional Microfluidic Cell Models. *Front. Physiol.* **2018**, *9*, 815. [[CrossRef](#)] [[PubMed](#)]
18. Luka, G.; Ahmadi, A.; Najjaran, H.; Alocilja, E.; DeRosa, M.; Wolthers, K.; Malki, A.; Aziz, H.; Althani, A.; Hoorfar, M. Microfluidics Integrated Biosensors: A Leading Technology towards Lab-on-a-Chip and Sensing Applications. *Sensors* **2015**, *15*, 30011–30031. [[CrossRef](#)] [[PubMed](#)]
19. Li, X.; Soler, M.; Szydzik, C.; Khoshmanesh, K.; Schmidt, J.; Coukos, G.; Mitchell, A.; Altug, H. Single Cell Analysis: Label-Free Optofluidic Nanobiosensor Enables Real-Time Analysis of Single-Cell Cytokine Secretion. *Small* **2018**, *14*, 1870119. [[CrossRef](#)]
20. Errico, V.; Ninno, A.D.; Bertani, F.R.; Businaro, L.; Bisegna, P.; Caselli, F. Mitigating positional dependence in coplanar electrode Coulter-type microfluidic devices. *Sens. Actuators B Chem.* **2017**, *247*, 580–586. [[CrossRef](#)]
21. Li, X.; Soler, M.; Szydzik, C.; Khoshmanesh, K.; Schmidt, J.; Coukos, G.; Mitchell, A.; Altug, H. Label-Free Optofluidic Nanobiosensor Enables Real-Time Analysis of Single-Cell Cytokine Secretion. *Small* **2018**, *14*, 1800698. [[CrossRef](#)]
22. Podwin, A.; Lizanets, D.; Przystupski, D.; Kubicki, W.; Śniadek, P.; Kulbacka, J.; Wymysłowski, A.; Walczak, R.; Dziuban, J.A. Lab-on-Chip Platform for Culturing and Dynamic Evaluation of Cells Development. *Micromachines* **2020**, *11*, 196. [[CrossRef](#)] [[PubMed](#)]
23. Schmid, Y.R.F.; Bürgel, S.C.; Misun, P.M.; Hierlemann, A.; Frey, O. Electrical Impedance Spectroscopy for Microtissue Spheroid Analysis in Hanging-Drop Networks. *ACS Sens.* **2016**, *1*, 1028–1035. [[CrossRef](#)] [[PubMed](#)]
24. Rezaei Kolahchi, A.; Khadem Mohtaram, N.; Pezeshgi Modarres, H.; Mohammadi, M.H.; Geraili, A.; Jafari, P.; Akbari, M.; Sanati-Nezhad, A. Microfluidic-Based Multi-Organ Platforms for Drug Discovery. *Micromachines* **2016**, *7*, 162. [[CrossRef](#)]
25. Lee, S.H.; Hong, S.; Song, J.; Cho, B.; Han, E.J.; Kondapavulur, S.; Kim, D.; Lee, L.P. Microphysiological Analysis Platform of Pancreatic Islet  $\beta$ -Cell Spheroids. *Adv. Healthc. Mater.* **2018**, *7*, 1701111. [[CrossRef](#)]
26. Järvinen, P.; Bonabi, A.; Jokinen, V.; Sikanen, T. Simultaneous Culturing of Cell Monolayers and Spheroids on a Single Microfluidic Device for Bridging the Gap between 2D and 3D Cell Assays in Drug Research. *Adv. Funct. Mater.* **2020**, *30*, 2000479. [[CrossRef](#)]
27. Zbinden, A.; Marzi, J.; Schlünder, K.; Probst, C.; Urbanczyk, M.; Black, S.; Brauchle, E.M.; Layland, S.L.; Kraushaar, U.; Duffy, G.; et al. Non-invasive marker-independent high content analysis of a microphysiological human pancreas-on-a-chip model. *Matrix Biol.* **2020**, *85*, 205–220. [[CrossRef](#)]

28. Saleheen, A.; Acharyya, D.; Prosser, R.A.; Baker, C.A. A microfluidic bubble perfusion device for brain slice culture. *Anal. Methods* **2021**, *13*, 1364–1373. [[CrossRef](#)] [[PubMed](#)]
29. Gong, J.; Meng, T.; Yang, J.; Hu, N.; Zhao, H.; Tian, T. Three-dimensional in vitro tissue culture models of brain organoids. *Exp. Neurol.* **2021**, *339*, 113619. [[CrossRef](#)]
30. Samiei, E.; Seyfoori, A.; Toyota, B.; Ghavami, S.; Akbari, M. Investigating Programmed Cell Death and Tumor Invasion in a Three-Dimensional (3D) Microfluidic Model of Glioblastoma. *Int. J. Mol. Sci.* **2020**, *21*, 3162. [[CrossRef](#)]
31. Wang, Y.; Wang, H.; Deng, P.; Tao, T.; Liu, H.; Wu, S.; Chen, W.; Qin, J. Modeling Human Nonalcoholic Fatty Liver Disease (NAFLD) with an Organoids-on-a-Chip System. *ACS Biomater. Sci. Eng.* **2020**, *6*, 5734–5743. [[CrossRef](#)]
32. Tronolone, J.J.; Jain, A. Engineering New Microvascular Networks On-Chip: Ingredients, Assembly, and Best Practices. *Adv. Funct. Mater.* **2021**, *31*, 2007199. [[CrossRef](#)] [[PubMed](#)]
33. Marrero, D.; Pujol-Vila, F.; Vera, D.; Gabriel, G.; Illa, X.; Elizalde-Torrent, A.; Alvarez, M.; Villa, R. Gut-on-a-chip: Mimicking and monitoring the human intestine. *Biosens. Bioelectron.* **2021**, *181*, 113156. [[CrossRef](#)]
34. Zheng, L.; Wang, B.; Sun, Y.; Dai, B.; Fu, Y.; Zhang, Y.; Wang, Y.; Yang, Z.; Sun, Z.; Zhuang, S.; et al. An Oxygen-Concentration-Controllable Multiorgan Microfluidic Platform for Studying Hypoxia-Induced Lung Cancer-Liver Metastasis and Screening Drugs. *ACS Sens.* **2021**, *6*, 823–832. [[CrossRef](#)]
35. Valente, K.P.; Thind, S.S.; Akbari, M.; Suleman, A.; Brolo, A.G. Collagen Type I-Gelatin Methacryloyl Composites: Mimicking the Tumor Microenvironment. *ACS Biomater. Sci. Eng.* **2019**, *5*, 2887–2898. [[CrossRef](#)]
36. Marconi, A.; Quadri, M.; Saltari, A.; Pincelli, C. Progress in melanoma modelling in vitro. *Exp. Dermatol.* **2018**, *27*, 578–586. [[CrossRef](#)] [[PubMed](#)]
37. Fetah, K.L.; DiPardo, B.J.; Kongadzem, E.-M.; Tomlinson, J.S.; Elzagheid, A.; Elmusrati, M.; Khademhosseini, A.; Ashammakhi, N. Cancer Modeling-on-a-Chip with Future Artificial Intelligence Integration. *Small* **2019**, *15*, 1901985. [[CrossRef](#)]
38. Clarke, G.A.; Hartse, B.X.; Niaraki Asli, A.E.; Taghavimehr, M.; Hashemi, N.; Abbasi Shirsavar, M.; Montazami, R.; Alimoradi, N.; Nasirian, V.; Ouedraogo, L.J.; et al. Advancement of Sensor Integrated Organ-on-Chip Devices. *Sensors* **2021**, *21*, 1367. [[CrossRef](#)]
39. Wang, X.-D.; Wolfbeis, O.S. Optical methods for sensing and imaging oxygen: Materials, spectroscopies and applications. *Chem. Soc. Rev.* **2014**, *43*, 3666–3761. [[CrossRef](#)]
40. Grist, S.M.; Chrostowski, L.; Cheung, K.C. Optical Oxygen Sensors for Applications in Microfluidic Cell Culture. *Sensors* **2010**, *10*, 9286–9316. [[CrossRef](#)]
41. Grate, J.W.; Liu, B.; Kelly, R.T.; Anheier, N.C.; Schmidt, T.M. Microfluidic Sensors with Impregnated Fluorophores for Simultaneous Imaging of Spatial Structure and Chemical Oxygen Gradients. *ACS Sens.* **2019**, *4*, 317–325. [[CrossRef](#)] [[PubMed](#)]
42. Matsumoto, S.; Safitri, A.R.; Danoy, M.; Maekawa, T.; Kinoshita, H.; Shinohara, M.; Sakai, Y.; Fujii, T.; Leclerc, E. Investigation of the hepatic respiration and liver zonation on rat hepatocytes using an integrated oxygen biosensor in a microscale device. *Biotechnol. Prog.* **2019**, *35*, e2854. [[CrossRef](#)]
43. Müller, B.; Sulzer, P.; Walch, M.; Zirath, H.; Buryška, T.; Rothbauer, M.; Ertl, P.; Mayr, T. Measurement of respiration and acidification rates of mammalian cells in thermoplastic microfluidic devices. *Sens. Actuators B Chem.* **2021**, *334*, 129664. [[CrossRef](#)]
44. Orcheston-Findlay, L.; Hashemi, A.; Garrill, A.; Nock, V. A microfluidic gradient generator to simulate the oxygen microenvironment in cancer cell culture. *Microelectron. Eng.* **2018**, *195*, 107–113. [[CrossRef](#)]
45. Ando, Y.; Ta, H.P.; Yen, D.P.; Lee, S.-S.; Raola, S.; Shen, K. A Microdevice Platform Recapitulating Hypoxic Tumor Microenvironments. *Sci. Rep.* **2017**, *7*, 15233. [[CrossRef](#)]
46. Huang, S.-H.; Huang, K.-S.; Liou, Y.-M. Simultaneous monitoring of oxygen consumption and acidification rates of a single zebrafish embryo during embryonic development within a microfluidic device. *Microfluid. Nanofluid.* **2016**, *21*, 3. [[CrossRef](#)]
47. Ehrlich, A.; Tsytkin-Kirschenschweig, S.; Ioannidis, K.; Ayyash, M.; Riu, A.; Note, R.; Ouedraogo, G.; Vanfleteren, J.; Cohen, M.; Nahmias, Y. Microphysiological flux balance platform unravels the dynamics of drug induced steatosis. *Lab Chip* **2018**, *18*, 2510–2522. [[CrossRef](#)]
48. Perottoni, S.; Neto, N.G.B.; Di Nitto, C.; Dmitriev, R.I.; Raimondi, M.T.; Monaghan, M.G. Intracellular label-free detection of mesenchymal stem cell metabolism within a perivascular niche-on-a-chip. *Lab Chip* **2021**, *21*, 1395–1408. [[CrossRef](#)]
49. Horka, M.; Sun, S.; Ruszczak, A.; Garstecki, P.; Mayr, T. Lifetime of Phosphorescence from Nanoparticles Yields Accurate Measurement of Concentration of Oxygen in Microdroplets, Allowing One To Monitor the Metabolism of Bacteria. *Anal. Chem.* **2016**, *88*, 12006–12012. [[CrossRef](#)] [[PubMed](#)]
50. Ehgartner, J.; Strobl, M.; Bolivar, J.M.; Rabl, D.; Rothbauer, M.; Ertl, P.; Borisov, S.M.; Mayr, T. Simultaneous Determination of Oxygen and pH Inside Microfluidic Devices Using Core-Shell Nanosensors. *Anal. Chem.* **2016**, *88*, 9796–9804. [[CrossRef](#)] [[PubMed](#)]
51. Lasave, L.C.; Borisov, S.M.; Ehgartner, J.; Mayr, T. Quick and simple integration of optical oxygen sensors into glass-based microfluidic devices. *RSC Adv.* **2015**, *5*, 70808–70816. [[CrossRef](#)]
52. Qiu, W.; Nagl, S. Automated Miniaturized Digital Microfluidic Antimicrobial Susceptibility Test Using a Chip-Integrated Optical Oxygen Sensor. *ACS Sens.* **2021**, *6*, 1147–1156. [[CrossRef](#)]
53. Gitlin, L.; Hoera, C.; Meier, R.J.; Nagl, S.; Belder, D. Micro flow reactor chips with integrated luminescent chemosensors for spatially resolved on-line chemical reaction monitoring. *Lab Chip* **2013**, *13*, 4134–4141. [[CrossRef](#)]
54. Grist, S.M.; Oyunerdene, N.; Flueckiger, J.; Kim, J.; Wong, P.C.; Chrostowski, L.; Cheung, K.C. Fabrication and laser patterning of polystyrene optical oxygen sensor films for lab-on-a-chip applications. *Analyst* **2014**, *139*, 5718–5727. [[CrossRef](#)] [[PubMed](#)]

55. Shaegh, S.A.M.; Ferrari, F.D.; Zhang, Y.S.; Nabavinia, M.; Mohammad, N.B.; Ryan, J.; Pourmand, A.; Laukaitis, E.; Sadeghian, R.B.; Nadhman, A.; et al. A microfluidic optical platform for real-time monitoring of pH and oxygen in microfluidic bioreactors and organ-on-chip devices. *Biomicrofluidics* **2016**, *10*, 044111. [[CrossRef](#)]
56. Yoon, H.K.; Lou, X.; Chen, Y.-C.; Koo Lee, Y.-E.; Yoon, E.; Kopelman, R. Nanophotosensitizers Engineered to Generate a Tunable Mix of Reactive Oxygen Species, for Optimizing Photodynamic Therapy, Using a Microfluidic Device. *Chem. Mater.* **2014**, *26*, 1592–1600. [[CrossRef](#)] [[PubMed](#)]
57. Pfeiffer, S.A.; Borisov, S.M.; Nagl, S. In-line monitoring of pH and oxygen during enzymatic reactions in off-the-shelf all-glass microreactors using integrated luminescent microsensors. *Microchim. Acta* **2017**, *184*, 621–626. [[CrossRef](#)]
58. Zhu, H.; Zhou, X.; Su, F.; Tian, Y.; Ashili, S.; Holl, M.R.; Meldrum, D.R. Micro-patterning and characterization of PHEMA-co-PAM-based optical chemical sensors for lab-on-a-chip applications. *Sens. Actuators B Chem.* **2012**, *173*, 817–823. [[CrossRef](#)] [[PubMed](#)]
59. Abdelgawad, M.; Freire, S.L.S.; Yang, H.; Wheeler, A.R. All-terrain droplet actuation. *Lab Chip* **2008**, *8*, 672–677. [[CrossRef](#)] [[PubMed](#)]
60. Lehner, P.; Staudinger, C.; Borisov, S.M.; Regensburger, J.; Klimant, I. Intrinsic Artefacts in Optical Oxygen Sensors—How Reliable are our Measurements? *Chem.—Eur. J.* **2015**, *21*, 3978–3986. [[CrossRef](#)] [[PubMed](#)]
61. Ungerböck, B.; Charwat, V.; Ertl, P.; Mayr, T. Microfluidic oxygen imaging using integrated optical sensor layers and a color camera. *Lab Chip* **2013**, *13*, 1593–1601. [[CrossRef](#)]
62. Bunge, F.; van den Driesche, S.; Waespy, M.; Radtke, A.; Belge, G.; Kelm, S.; Waite, A.M.; Mirastschijski, U.; Vellekoop, M.J. Microfluidic oxygen sensor system as a tool to monitor the metabolism of mammalian cells. *Sens. Actuators B Chem.* **2019**, *289*, 24–31. [[CrossRef](#)]
63. Rivera, K.R.; Pozdin, V.A.; Young, A.T.; Erb, P.D.; Wisniewski, N.A.; Magness, S.T.; Daniele, M. Integrated phosphorescence-based photonic biosensor (iPOB) for monitoring oxygen levels in 3D cell culture systems. *Biosens. Bioelectron.* **2019**, *123*, 131–140. [[CrossRef](#)]
64. Zhao, Y.; Liu, L.; Luo, T.; Hong, L.; Peng, X.; Austin, R.H.; Qu, J. A platinum-porphine/poly(perfluoroether) film oxygen tension sensor for noninvasive local monitoring of cellular oxygen metabolism using phosphorescence lifetime imaging. *Sens. Actuators B Chem.* **2018**, *269*, 88–95. [[CrossRef](#)]
65. Mazetyte-Stasinskiene, R.; Köhler, J.M. Sensor Micro and Nanoparticles for Microfluidic Application. *Appl. Sci.* **2020**, *10*, 8353. [[CrossRef](#)]
66. Li, B.; Zhao, Y.; Zhang, Y.; Zhang, A.; Li, X.; Gu, J.; Xi, S.; Zhou, G. Functionalized Micro Structured Optical Fibers and Devices for Sensing Applications: A Review. *J. Lightw. Technol.* **2021**, *39*, 3812–3823. [[CrossRef](#)]
67. Yang, X.; Zheng, Y.; Luo, S.; Liu, Y.; Yuan, L. Microfluidic in-fiber oxygen sensor derivates from a capillary optical fiber with a ring-shaped waveguide. *Sens. Actuators B Chem.* **2013**, *182*, 571–575. [[CrossRef](#)]
68. Jiang, K.; Thomas, P.C.; Forry, S.P.; DeVoe, D.L.; Raghavan, S.R. Microfluidic synthesis of monodisperse PDMS microbeads as discrete oxygen sensors. *Soft Matter* **2012**, *8*, 923–926. [[CrossRef](#)]
69. Bavli, D.; Prill, S.; Ezra, E.; Levy, G.; Cohen, M.; Vinken, M.; Vanfleteren, J.; Jaeger, M.; Nahmias, Y. Real-time monitoring of metabolic function in liver-on-chip microdevices tracks the dynamics of mitochondrial dysfunction. *Proc. Natl. Acad. Sci. USA* **2016**, *113*, E2231–E2240. [[CrossRef](#)]
70. Tanumihardja, E.; Olthuis, W.; Van den Berg, A. Ruthenium Oxide Nanorods as Potentiometric pH Sensor for Organs-On-Chip Purposes. *Sensors* **2018**, *18*, 2901. [[CrossRef](#)] [[PubMed](#)]
71. Wang, X.-H.; Peng, H.-S.; Chang, Z.; Hou, L.-L.; You, F.-T.; Teng, F.; Song, H.-W.; Dong, B. Synthesis of ratiometric fluorescent nanoparticles for sensing oxygen. *Microchim. Acta* **2012**, *178*, 147–152. [[CrossRef](#)]
72. Cao, J.; Nagl, S.; Kothe, E.; Köhler, J.M. Oxygen sensor nanoparticles for monitoring bacterial growth and characterization of dose-response functions in microfluidic screenings. *Microchim. Acta* **2015**, *182*, 385–394. [[CrossRef](#)]
73. Li, Y.-C.E.; Lee, I.-C. The Current Trends of Biosensors in Tissue Engineering. *Biosensors* **2020**, *10*, 88. [[CrossRef](#)]
74. Yoon, J.; Shin, M.; Lee, T.; Choi, J.-W. Highly Sensitive Biosensors Based on Biomolecules and Functional Nanomaterials Depending on the Types of Nanomaterials: A Perspective Review. *Materials* **2020**, *13*, 299. [[CrossRef](#)]
75. Naresh, V.; Lee, N. A Review on Biosensors and Recent Development of Nanostructured Materials-Enabled Biosensors. *Sensors* **2021**, *21*, 1109. [[CrossRef](#)]
76. Ungerböck, B.; Fellinger, S.; Sulzer, P.; Abel, T.; Mayr, T. Magnetic optical sensor particles: A flexible analytical tool for microfluidic devices. *Analyst* **2014**, *139*, 2551–2559. [[CrossRef](#)] [[PubMed](#)]
77. Zhu, F.; Baker, D.; Skommer, J.; Sewell, M.; Wlodkovic, D. Real-time 2D visualization of metabolic activities in zebrafish embryos using a microfluidic technology. *Cytom. Part A* **2015**, *87*, 446–450. [[CrossRef](#)]
78. Ehgartner, J.; Sulzer, P.; Burger, T.; Kasjanow, A.; Bouwes, D.; Krühne, U.; Klimant, I.; Mayr, T. Online analysis of oxygen inside silicon-glass microreactors with integrated optical sensors. *Sens. Actuators B Chem.* **2016**, *228*, 748–757. [[CrossRef](#)]
79. Xu, X.; Koivisto, O.; Liu, C.; Zhou, J.; Miihkinen, M.; Jacquemet, G.; Wang, D.; Rosenholm, J.M.; Shu, Y.; Zhang, H. Effective Delivery of the CRISPR/Cas9 System Enabled by Functionalized Mesoporous Silica Nanoparticles for GFP-Tagged Paxillin Knock-In. *Adv. Ther.* **2021**, *4*. [[CrossRef](#)]
80. Wang, F.; Chen, L.; Zhu, J.; Hu, X.; Yang, Y. A Phosphorescence Quenching-Based Intelligent Dissolved Oxygen Sensor on an Optofluidic Platform. *Micromachines* **2021**, *12*, 281. [[CrossRef](#)]

81. Park, J.; Nam, H.; Ahn, S.Y.; Pak, Y.K.; Pak, J.J. A reservoir-type oxygen sensor with  $2 \times 3$  array for measuring cellular respiration levels. *Sens. Actuators B Chem.* **2013**, *176*, 913–920. [[CrossRef](#)]
82. Mestres, P.; Morguet, A. The Bionas technology for anticancer drug screening. *Expert Opin. Drug Discov.* **2009**, *4*, 785–797. [[CrossRef](#)]
83. Wu, C.-C.; Yasukawa, T.; Shiku, H.; Matsue, T. Fabrication of miniature Clark oxygen sensor integrated with microstructure. *Sens. Actuators B Chem.* **2005**, *110*, 342–349. [[CrossRef](#)]
84. Luo, J.; Dziubla, T.; Eitel, R. A low temperature co-fired ceramic based microfluidic Clark-type oxygen sensor for real-time oxygen sensing. *Sens. Actuators B Chem.* **2017**, *240*, 392–397. [[CrossRef](#)]
85. Liebisch, F.; Weltin, A.; Marzioch, J.; Urban, G.A.; Kieninger, J. Zero-consumption Clark-type microsensor for oxygen monitoring in cell culture and organ-on-chip systems. *Sens. Actuators B Chem.* **2020**, *322*, 128652. [[CrossRef](#)]
86. Moya, A.; Illa, X.; Gimenez, I.; Lazo-Fernandez, Y.; Villa, R.; Errachid, A.; Gabriel, G. Miniaturized multiparametric flexible platform for the simultaneous monitoring of ionic: Application in real urine. *Sens. Actuators B Chem.* **2018**, *255*, 2861–2870. [[CrossRef](#)]
87. Bonk, S.M.; Stubbe, M.; Buehler, S.M.; Tautorat, C.; Baumann, W.; Klinkenberg, E.D.; Gimsa, J. Design and Characterization of a Sensorized Microfluidic Cell-Culture System with Electro-Thermal Micro-Pumps and Sensors for Cell Adhesion, Oxygen, and pH on a Glass Chip. *Biosensors* **2015**, *5*, 513–536. [[CrossRef](#)]
88. Weltin, A.; Slotwinski, K.; Kieninger, J.; Moser, I.; Jobst, G.; Wego, M.; Ehret, R.; Urban, G.A. Cell culture monitoring for drug screening and cancer research: A transparent, microfluidic, multi-sensor microsystem. *Lab Chip* **2014**, *14*, 138–146. [[CrossRef](#)]
89. Pereira Rodrigues, N.; Sakai, Y.; Fujii, T. Cell-based microfluidic biochip for the electrochemical real-time monitoring of glucose and oxygen. *Sens. Actuators B Chem.* **2008**, *132*, 608–613. [[CrossRef](#)]
90. Li, C.; Wu, P.-M.; Jung, W.; Ahn, C.H.; Shutter, L.A.; Narayan, R.K. A novel lab-on-a-tube for multimodality neuromonitoring of patients with traumatic brain injury (TBI). *Lab Chip* **2009**, *9*, 1988–1990. [[CrossRef](#)] [[PubMed](#)]
91. Sekli Belaïdi, F.; Salvagnac, L.; Assié Souleille, S.; Blatché, M.C.; Bedel-Pereira, E.; Séguy, I.; Temple-Boyer, P.; Launay, J. Accurate physiological monitoring using lab-on-a-chip platform for aquatic micro-organisms growth and optimized culture. *Sens. Actuators B Chem.* **2020**, *321*, 128492. [[CrossRef](#)]
92. Van Rossem, F.; Bomer, J.G.; de Boer, H.L.; Abbas, Y.; de Weerd, E.; van den Berg, A.; Le Gac, S. Sensing oxygen at the millisecond time-scale using an ultra-microelectrode array (UMEA). *Sens. Actuators B Chem.* **2017**, *238*, 1008–1016. [[CrossRef](#)]
93. Vonau, W.; Gerlach, F.; Herrmann, S. Conception of a new technique in cell cultivation using a lab-on-chip aided miniaturised device with calibratable electrochemical sensors. *Microchim. Acta* **2010**, *171*, 451–456. [[CrossRef](#)]
94. Moya, A.; Ortega-Ribera, M.; Guimerà, X.; Sowade, E.; Zea, M.; Illa, X.; Ramon, E.; Villa, R.; Gracia-Sancho, J.; Gabriel, G. Online oxygen monitoring using integrated inkjet-printed sensors in a liver-on-a-chip system. *Lab Chip* **2018**, *18*, 2023–2035. [[CrossRef](#)]
95. Weltin, A.; Hammer, S.; Noor, F.; Kaminski, Y.; Kieninger, J.; Urban, G.A. Accessing 3D microtissue metabolism: Lactate and oxygen monitoring in hepatocyte spheroids. *Biosens. Bioelectron.* **2017**, *87*, 941–948. [[CrossRef](#)]
96. Alexander, F., Jr.; Eggert, S.; Wiest, J. A novel lab-on-a-chip platform for spheroid metabolism monitoring. *Cytotechnology* **2018**, *70*, 375–386. [[CrossRef](#)]
97. Yang, Z.; Suzuki, H.; Sasaki, S.; Karube, I. Disposable sensor for biochemical oxygen demand. *Appl. Microbiol. Biotechnol.* **1996**, *46*, 10–14. [[CrossRef](#)]
98. Mehta, G.; Mehta, K.; Sud, D.; Song, J.W.; Bersano-Begey, T.; Futai, N.; Heo, Y.S.; Mycek, M.A.; Linderman, J.J.; Takayama, S. Quantitative measurement and control of oxygen levels in microfluidic poly(dimethylsiloxane) bioreactors during cell culture. *Biomed. Microdevices* **2007**, *9*, 123–134. [[CrossRef](#)]
99. Suzuki, H.; Sugama, A.; Kojima, N. Micromachined Clark oxygen electrode. *Sens. Actuators B Chem.* **1993**, *10*, 91–98. [[CrossRef](#)]
100. Gongora-Rubio, M.R.; Espinoza-Vallejos, P.; Sola-Laguna, L.; Santiago-Avilés, J.J. Overview of low temperature co-fired ceramics tape technology for meso-system technology (MsST). *Sens. Actuators A Phys.* **2001**, *89*, 222–241. [[CrossRef](#)]
101. Jurkó, D.; Maeder, T.; Dąbrowski, A.; Zarnik, M.S.; Belavič, D.; Bartsch, H.; Müller, J. Overview on low temperature co-fired ceramic sensors. *Sens. Actuators A Phys.* **2015**, *233*, 125–146. [[CrossRef](#)]
102. Brandenburg, A.; Wappler, E.; Kita, J.; Moos, R. Miniaturized ceramic DSC device with strain gauge-based mass detection—First steps to realize a fully integrated DSC/TGA device. *Sens. Actuators A Phys.* **2016**, *241*, 145–151. [[CrossRef](#)]
103. Ross, J.J.W. Method and Apparatus for Electrolytically Determining a Species in a Fluid. U.S. Patent 3,260,656, 12 July 1966.
104. Bonk, S.M.; Oldorf, P.; Peters, R.; Baumann, W.; Gimsa, J. Fast Prototyping of Sensorized Cell Culture Chips and Microfluidic Systems with Ultrashort Laser Pulses. *Micromachines* **2015**, *6*, 364–374. [[CrossRef](#)]
105. Sticker, D.; Rothbauer, M.; Ehgartner, J.; Steininger, C.; Liske, O.; Liska, R.; Neuhaus, W.; Mayr, T.; Haraldsson, T.; Kutter, J.P.; et al. Oxygen Management at the Microscale: A Functional Biochip Material with Long-Lasting and Tunable Oxygen Scavenging Properties for Cell Culture Applications. *ACS Appl. Mater. Interfaces* **2019**, *11*, 9730–9739. [[CrossRef](#)]
106. Estrada-Leypon, O.; Moya, A.; Guimera, A.; Gabriel, G.; Agut, M.; Sanchez, B.; Borros, S. Simultaneous monitoring of *Staphylococcus aureus* growth in a multi-parametric microfluidic platform using microscopy and impedance spectroscopy. *Bioelectrochemistry* **2015**, *105*, 56–64. [[CrossRef](#)]
107. Mitrovski, S.M.; Nuzzo, R.G. An electrochemically driven poly(dimethylsiloxane) microfluidic actuator: Oxygen sensing and programmable flows and pH gradients. *Lab Chip* **2005**, *5*, 634–645. [[CrossRef](#)]

108. Furlani, D.; Li, W.; Pittermann, E.; Klopsch, C.; Wang, L.; Knopp, A.; Jungebluth, P.; Thedinga, E.; Havenstein, C.; Westien, I.; et al. A Transformed Cell Population Derived from Cultured Mesenchymal Stem Cells has no Functional Effect after Transplantation into the Injured Heart. *Cell Transplant.* **2009**, *18*, 319–332. [[CrossRef](#)]
109. Thedinga, E.; Kob, A.; Holst, H.; Keuer, A.; Drechsler, S.; Niendorf, R.; Baumann, W.; Freund, I.; Lehmann, M.; Ehret, R. Online monitoring of cell metabolism for studying pharmacodynamic effects. *Toxicol. Appl. Pharmacol.* **2007**, *220*, 33–44. [[CrossRef](#)]
110. Thedinga, E.; Ullrich, A.; Drechsler, S.; Niendorf, R.; Kob, A.; Runge, D.; Keuer, A.; Freund, I.; Lehmann, M.; Ehret, R. In vitro system for the prediction of hepatotoxic effects in primary hepatocytes. *Altox* **2007**, *24*, 22–34. [[CrossRef](#)]
111. Yao, J.; Guan, Y.; Park, Y.; Choi, Y.E.; Kim, H.S.; Park, J. Optimization of PTFE Coating on PDMS Surfaces for Inhibition of Hydrophobic Molecule Absorption for Increased Optical Detection Sensitivity. *Sensors* **2021**, *21*, 1754. [[CrossRef](#)]
112. Wang, L.; Liu, W.; Wang, Y.; Wang, J.C.; Tu, Q.; Liu, R.; Wang, J. Construction of oxygen and chemical concentration gradients in a single microfluidic device for studying tumor cell-drug interactions in a dynamic hypoxia microenvironment. *Lab Chip* **2013**, *13*, 695–705. [[CrossRef](#)]
113. Lo, J.F.; Sinkala, E.; Eddington, D.T. Oxygen gradients for open well cellular cultures via microfluidic substrates. *Lab Chip* **2010**, *10*, 2394–2401. [[CrossRef](#)]
114. Moya, A.; Sowade, E.; del Campo, F.J.; Mitra, K.Y.; Ramon, E.; Villa, R.; Baumann, R.R.; Gabriel, G. All-inkjet-printed dissolved oxygen sensors on flexible plastic substrates. *Org. Electron.* **2016**, *39*, 168–176. [[CrossRef](#)]
115. Eklund, S.E.; Taylor, D.; Kozlov, E.; Prokop, A.; Cliffl, D.E. A Microphysiometer for Simultaneous Measurement of Changes in Extracellular Glucose, Lactate, Oxygen, and Acidification Rate. *Anal. Chem.* **2004**, *76*, 519–527. [[CrossRef](#)]
116. McKenzie, J.R.; Cognata, A.C.; Davis, A.N.; Wikswo, J.P.; Cliffl, D.E. Real-Time Monitoring of Cellular Bioenergetics with a Multianalyte Screen-Printed Electrode. *Anal. Chem.* **2015**, *87*, 7857–7864. [[CrossRef](#)]
117. Hafner, F. Cytosensor Microphysiometer: Technology and recent applications. *Biosens. Bioelectron.* **2000**, *15*, 149–158. [[CrossRef](#)]
118. Lehmann, M.; Baumann, W.; Brischwein, M.; Ehret, R.; Kraus, M.; Schwinde, A.; Bitzenhofer, M.; Freund, I.; Wolf, B. Non-invasive measurement of cell membrane associated proton gradients by ion-sensitive field effect transistor arrays for microphysiological and bioelectronic applications. *Biosens. Bioelectron.* **2000**, *15*, 117–124. [[CrossRef](#)]
119. Buehler, S.M.; Stubbe, M.; Gimsa, U.; Baumann, W.; Gimsa, J. A decrease of intracellular ATP is compensated by increased respiration and acidification at sub-lethal parathion concentrations in murine embryonic neuronal cells: Measurements in metabolic cell-culture chips. *Toxicol. Lett.* **2011**, *207*, 182–190. [[CrossRef](#)]
120. Koester, P.J.; Buehler, S.M.; Stubbe, M.; Tautorat, C.; Niendorf, M.; Baumann, W.; Gimsa, J. Modular glass chip system measuring the electric activity and adhesion of neuronal cells—Application and drug testing with sodium valproic acid. *Lab Chip* **2010**, *10*, 1579–1586. [[CrossRef](#)]
121. Torrents, A.; Mas, J.; Muñoz, F.X.; del Campo, F.J. Design of a microfluidic respirometer for semi-continuous amperometric short time biochemical oxygen demand (BOD<sub>st</sub>) analysis. *Biochem. Eng. J.* **2012**, *66*, 27–37. [[CrossRef](#)]
122. Edmondson, R.; Broglie, J.J.; Adcock, A.F.; Yang, L. Three-dimensional cell culture systems and their applications in drug discovery and cell-based biosensors. *Assay Drug Dev. Technol.* **2014**, *12*, 207–218. [[CrossRef](#)]